

PAPER • OPEN ACCESS

Magnonic crystals for data processing

To cite this article: A V Chumak *et al* 2017 *J. Phys. D: Appl. Phys.* **50** 244001

View the [article online](#) for updates and enhancements.

You may also like

- [Review and prospects of magnonic crystals and devices with reprogrammable band structure](#)
M Krawczyk and D Grundler
- [Spin-wave propagation through a magnonic crystal in a thermal gradient](#)
Thomas Langner, Dmytro A Bozhko, Sergiy A Bunyaev *et al.*
- [Tunable dispersion relations manipulated by strain in skyrmion-based magnonic crystals](#)
Zhao-Nian Jin, , Xuan-Lin He *et al.*



ECS
The
Electrochemical
Society
Advancing solid state &
electrochemical science & technology

DISCOVER
how sustainability
intersects with
electrochemistry & solid
state science research

Magnonic crystals for data processing

A V Chumak, A A Serga and B Hillebrands

Fachbereich Physik and Landesforschungszentrum OPTIMAS, Technische Universität Kaiserslautern, 67663 Kaiserslautern, Germany

E-mail: chumak@physik.uni-kl.de

Received 13 February 2017

Accepted for publication 31 March 2017

Published 23 May 2017



CrossMark

Abstract

Magnons (the quanta of spin waves) propagating in magnetic materials with wavelengths at the nanometer-scale and carrying information in the form of an angular momentum can be used as data carriers in next-generation, nano-sized low-loss information processing systems. In this respect, artificial magnetic materials with properties periodically varied in space, known as magnonic crystals, are especially promising for controlling and manipulating magnon currents. In this article, different approaches for the realization of static, reconfigurable, and dynamic magnonic crystals are presented along with a variety of novel wave phenomena discovered in these crystals. Special attention is devoted to the utilization of magnonic crystals for processing of analog and digital information.

Keywords: magnonic crystals, magnonics, magnon spintronics, spin-wave physics, artificial media

(Some figures may appear in colour only in the online journal)

1. Introduction

This article focuses on a selection of results in the field of magnonic crystals obtained within the last decade in our group. Special attention is devoted to the application of magnonic crystals in data processing and information technologies. Because of the large number of achievements in the field, it is unavoidable that many important results are excluded from this article. Therefore, we would like to direct the reader's attention to excellent reviews devoted to different aspects of magnonic crystals: spin-wave dynamics in periodic structures for microwave applications [1, 2], Brillouin light scattering (BLS) studies of planar metallic magnonic crystals [3], micromagnetic computer simulations of width-modulated waveguides [4], photo-magnonic aspects of antidot lattices studies [5], theoretical studies of one-dimensional monomode waveguides [6], and reconfigurable magnonic crystals [7]. The results presented in the current review were already partially presented in our own reviews of *yttrium iron garnet (YIG) magnonics* [8] and *magnon spintronics* [9] as well as

in book chapters on dynamic magnonic crystals [10] and magnon spintronics [11].

The article is organized in the following way: In the introduction we describe the field of magnon spintronics and discuss the role of magnonic crystals in it. The next section 2 is devoted to the properties of spin waves in thin planar films and waveguides, to the magnetic materials commonly used in the field, and to the methods of spin-wave excitation and detection. Sections 3 and 4 are devoted to the study of physical phenomena taking place in static and dynamic magnonic crystals, respectively. The application of magnonic crystals for magnon-based processing of analog and digital data is discussed in section 5. Specifically, static magnonic crystals can be used as passive elements, like microwave filters, resonators or delay lines for microwave generation. Reconfigurable and dynamic magnonic crystals are promising as active devices performing, for example, tunable filtering, frequency conversion or time reversal. In the final section we briefly summarize the results.

1.1. Magnon spintronics: from electron- to magnon-based computing

A disturbance in the local magnetic order can propagate in a magnetic material in the form of a wave. This wave was first predicted by Bloch in 1929 and was named spin wave since

 Original content from this work may be used under the terms of the [Creative Commons Attribution 3.0 licence](https://creativecommons.org/licenses/by/3.0/). Any further distribution of this work must maintain attribution to the author(s) and the title of the work, journal citation and DOI.

it is related to a collective excitation of the electron spin system in ferromagnetic metals and insulators [12]. Since that time, the field of magnetization dynamics has grown into a wide domain of science in which studies of coherent externally driven spin waves are of particular importance. Spin-wave characteristics can be engineered by a wide range of parameters, including the choice of magnetic material, the shape of the sample and the orientation and size of the applied biasing magnetic field [13, 14]. This, in combination with a rich choice of linear and nonlinear spin-wave properties, makes spin waves excellent objects of study in general wave physics [8]. One- and two-dimensional soliton formation [15, 16], nondiffractive spin-wave caustic beams [17–19], wave-front reversals [20, 21], room-temperature Bose–Einstein condensation (BEC) of magnons [22, 23], and formation of magnon supercurrents [24] are just a small selection of examples.

On the other hand, spin waves in the GHz frequency range are of great interest for applications in telecommunication systems and radars since spin-wave wavelengths are orders of magnitude shorter than those of electromagnetic waves, opening up access to the miniaturization of analog data processing elements. Nowadays, spin waves and their quanta, magnons, also attract much attention due to another very ambitious perspective: They are being considered as data carriers in novel computing devices instead of electrons in electronics. The main advantages offered by magnons for data processing are [9, 25]:

- Potential for realizing novel, highly efficient, wave-based computing concepts.
- Spin waves can be used in devices of sizes down to sub-10 nm.
- Magnon frequencies cover a very wide range from sub-gigahertz to tens of tetrahertz.
- Magnons allow for the room-temperature transport of spin information without the translational motion of electrons and, therefore, without the generation of parasitic joule heat.
- Pronounced spin-wave nonlinear effects allow for the realization of magnon–magnon interaction-based functionalities, such as signal gating in a magnon transistor.

The field of science that refers to information transport and processing by spin waves is known as magnonics [5, 8, 26, 27]. The utilization of magnonic approaches in the field of spintronics, hitherto addressing electron-based spin currents, gave birth to the field of magnon spintronics [9, 25]. The diagram of magnon spintronics in figure 1 shows that, besides magnon-based elements operating with analog and digital data, this field also comprises converters between the magnon subsystem and electron-based spin and charge currents. Different approaches, including utilization of spin transfer torque, spin Hall effect, magneto-acoustic phenomena, opto-magnetic phenomena, and many others, are currently under intensive investigation. The converters are outside the scope of the article but are partially presented in the review [9].

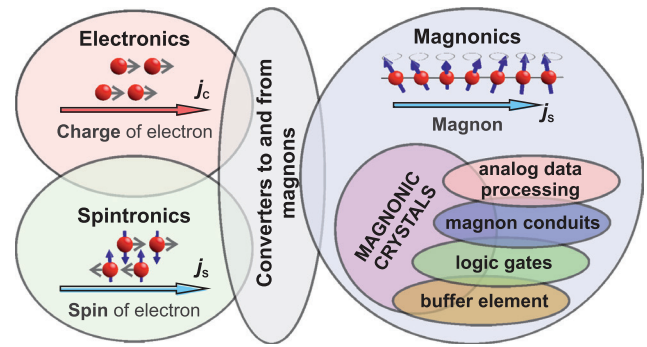


Figure 1. The concept of magnon spintronics. Data coded in charge or spin currents are converted to magnon currents, processed within the magnonic system and converted back. The magnonic crystal is a universal element in the field of magnonics which can be used for data transfer, processing, and buffering.

1.2. Magnonic crystals and their role in the field of magnon spintronics

Magnonic crystals, which are artificial magnetic media with properties characterized by periodic lateral variation, are of great interest in both pure wave physics and application-oriented magnonics. The spectra of spin-wave excitations in such structures are significantly different from those in uniform media and exhibit features such as band gaps, where spin waves are not allowed to propagate. In spite of the fact that the term ‘magnonic crystal’ is relatively new (it was introduced by Nikitov *et al* in 2001 [28]), this field goes back to studies of spin-wave propagation in periodical structures which were initiated by Sykes, Adam and Collins in 1976 [29]. Early magnonic crystal research activity was mainly restricted by application to the development of microwave filters and resonators—see reviews [1, 2, 30].

Nowadays, when the linear and nonlinear coupling of spin-wave modes and demagnetizing effects cannot be neglected on the nano- and micro-scale, many studies are focused on understanding spin-wave-related physical phenomena in magnonic crystals. In particular, considerable attention has attracted investigations of magnonic crystals with defects [31–35], topological and nonreciprocal phenomena in magnonic crystals [36–44], linear and nonlinear spin-wave dynamics in coupled magnonic crystals [45–47], and the formation and propagation of solitons [48–51]. Besides one-dimensional magnonic crystals [81–98], two-dimensional magnonic crystals [52–77] have been intensively studied experimentally while three-dimensional magnonic crystals [78–80] are investigated theoretically. Thus, the magnonic crystal field is growing fast. For magnon spintronic applications, magnonic crystals constitute one of the key elements since they open up access to novel multi-functional magnonic devices [9]. These devices can be used as spin-wave conduits and filters (we do not provide any citations here since, in fact, any magnonic crystal can serve as a conduit or a filter), sensors [99–101], delay lines and phase shifters [102, 103], components of auto-oscillators [49, 51, 102, 103], frequency and time inverters [104, 105], data-buffering elements [105, 106], power limiters [107], nonlinear enhancers in a magnon transistor [108], and components of logic gates [109, 110].

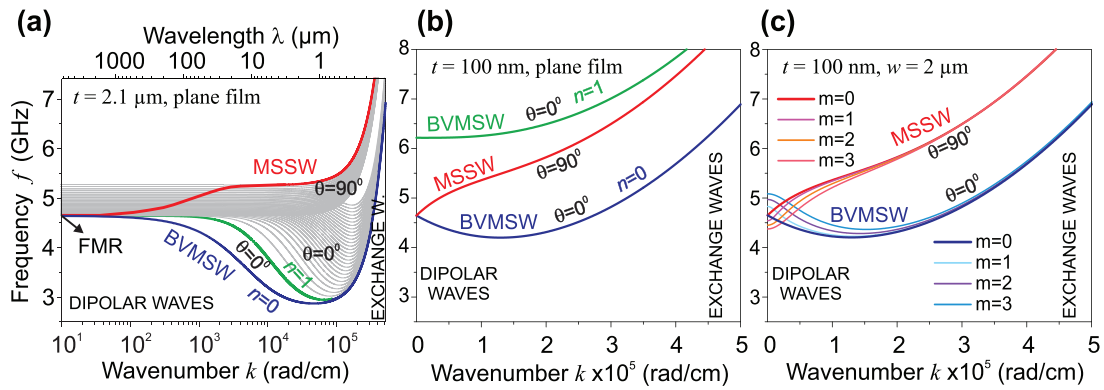


Figure 2. Spin-wave dispersion characteristics for an infinite in-plane magnetized yttrium iron garnet (YIG) film of $2.1 \mu\text{m}$ thickness (a), an infinite film of 100 nm thickness (b), and a $2 \mu\text{m}$ wide spin-wave waveguide of 100 nm thickness (c). A magnetic field of 100 mT is applied in-plane, the saturation magnetization is 140 kA m^{-1} , the exchange constant is 3.6 pJ m^{-1} , and θ is the angle between the spin-wave propagation direction and the magnetization. (a) Logarithmic scale is used for the wavenumber. The blue line shows the lowest $n = 0$ thickness mode of a backward-volume magnetostatic wave (BVMSW) propagating along the magnetic field; the green line shows the first $n = 1$ BVMSW thickness mode and the red line shows the magnetostatic surface spin wave (MSSW) propagating transversely to the orientation of the magnetic field. Twenty-nine higher-order thickness modes are shown in gray. The dispersions were found by numerical calculations using the approach developed in [112–114]. (b) A linear scale is used for the wavenumber. The dispersions for the MSSW as well as zero $n = 0$ and first $n = 1$ BVMSW modes are shown. (c) The dispersions for the zero thickness mode $n = 0$ with different width modes m are shown. The calculations in (b) and (c) are performed using the simplified analytical expressions in [113], additionally accounting for the width modes $k_{\text{SUM}}^2 = k^2 + (m\pi/w)^2$ and the dependence of the spin-wave propagation angle on the width mode $\phi(w, m)$.

2. Essentials of spin-wave dynamics

2.1. Spin waves in thin magnetic films and waveguides

Spin waves are related to a collective excitation of the electron spin system in ferromagnetic metals and insulators (see books [13, 14]). The main spin-wave characteristics can be obtained from analysis of the dispersion relation, i.e. the dependence of the wave frequency f on the wavenumber k . There are two main contributors to the magnon energy: long-range dipole–dipole and short-range exchange interactions. As a result, the dispersions of spin waves are significantly different from the well-known dispersion of light or sound in uniform media. Moreover, spin-wave dispersion relations in in-plane magnetized films are strongly anisotropic due to the given orientation of the magnetization of the magnetic medium. Therefore, for example, spin waves propagating along the magnetization direction have a different dispersion from waves propagating transversely to the magnetization (see figure 2) [111].

In most practical situations spin waves are studied in spatially confined samples such as thin films or strips magnetized in-plane by an external magnetic field. The geometry of a spin-wave waveguide, namely its thickness and its width, is a key parameter defining the spin-wave dispersion along with the magnetic properties of the material and the applied magnetic field. In order to underline the role of the waveguide geometry, the dispersion relations for infinite-plane films of different thicknesses as well as for a spin-wave waveguide are shown in figure 2.

The typical spin-wave dispersion characteristics for an in-plane magnetized YIG film of micrometer thickness are shown in figure 2(a). In spite of the fact that spin waves can propagate at any angle θ relative to the magnetization orientation, only the dispersions for the cases of longitudinal

($\theta = 0^\circ$) and transverse ($\theta = 90^\circ$) wave propagation are shown for simplicity. The spectrum comprises three main regions: the region of small wavenumbers $k < 10^4 \text{ rad cm}^{-1}$ corresponds to dipolar waves, usually termed magnetostatic waves; the region of high $k > 10^5 \text{ rad cm}^{-1}$ corresponds to exchange waves; and the region in between corresponds to dipolar-exchange spin waves. One can see that, as opposed to the case presented in figures 2(b) and (c), the dispersions for the micrometer-thick YIG film show (i) a large decrease in the frequency of the backward-volume magnetostatic wave (BVMSW) mode to well below the ferromagnetic resonance (FMR) frequency, and (ii) a high density of higher-order thickness BVMSW modes, which are shown in gray. Please note that the magnetostatic surface spin wave (MSSW) mode has a hyperbolic rather than a cosine distribution of dynamic magnetization across the film thickness and, therefore, does not possess higher-order thickness modes. The complexity of the spectrum plays a crucial role in heavily overpopulated nonlinear magnonic systems and, for example, might result in the BEC of magnons [22, 23], in the generation of magnon supercurrents [24], and in effective nonlinear magnon scattering in a magnon transistor [108].

In contrast, the spin-wave spectrum of a thin film is significantly diluted, and only the first thickness mode is shown in figure 2(b) (the thickness modes not shown here have much higher frequencies). This is due to the fact that quantization across the film thickness results in an increase in the spin-wave frequency caused by exchange interaction. Figure 2(c) shows how the spin-wave quantization along the width of a waveguide changes the dispersion relations. One can see that the quantization of the modes across the waveguide results in a pronounced modification of the dispersion characteristics in the dipolar region. The short-wavelength exchange waves are much less sensitive to the geometry of the waveguide.

Table 1. Selection of magnetic materials for magnonic applications, their main parameters, and their estimated spin-wave characteristics. The characteristics are calculated using the dipolar approximation for infinite films magnetized in-plane with a 100 mT magnetic field. Magnetostatic surface spin waves that propagate perpendicularly to the magnetization direction and have the highest group velocities are considered. For simplicity, the spin wave of wavenumber $k = 0.1/t$ is analyzed. Lifetime is estimated using the bulk material approach without taking ellipticity into account [14].

	μm -thick LPE yttrium iron garnet (YIG)	nm-thick yttrium iron garnet (YIG)	Permalloy (Py)	CoFeB	Heusler CMFS compound
Chemical composition	$\text{Y}_3\text{Fe}_5\text{O}_{12}$	$\text{Y}_3\text{Fe}_5\text{O}_{12}$	$\text{Ni}_{81}\text{Fe}_{19}$	$\text{Co}_{40}\text{Fe}_{40}\text{B}_{20}$	$\text{Co}_2\text{Mn}_{0.6}\text{Fe}_{0.4}\text{Si}$
Structure	Single-crystal	Single-crystal	Amorphous	Amorphous	Single-crystal
Gilbert damping α	$5 \cdot 10^{-5}$	$2 \cdot 10^{-4}$	$7 \cdot 10^{-3}$	$4 \cdot 10^{-3}$	$3 \cdot 10^{-3}$
Saturation magnetization M_0	140 kA m $^{-1}$	140 kA m $^{-1}$	800 kA m $^{-1}$	1250 kA m $^{-1}$	1000 kA m $^{-1}$
Exchange constant A	3.6 pJ m $^{-1}$	3.6 pJ m $^{-1}$	16 pJ m $^{-1}$	15 pJ m $^{-1}$	13 pJ m $^{-1}$
Curie temperature T_C	560 K	560 K	550–870 K	1000 K	>985 K
Typical film thickness t	1–20 μm	5–100 nm	5–100 nm	5–100 nm	5–100 nm
Lifetime for MSSW	417 ns (@ 4.77 GHz)	167 ns (@ 4.77 GHz)	2.1 ns (@ 11.1 GHz)	2.7 ns (@ 14.8 GHz)	4.1 ns (@ 12.8 GHz)
Velocity v_{gr}	33.8 km s $^{-1}$ (@ $t = 5 \mu\text{m}$)	0.14 km s $^{-1}$ (@ $t = 20 \text{ nm}$)	1.9 km s $^{-1}$ (@ $t = 20 \text{ nm}$)	3.5 km s $^{-1}$ (@ $t = 20 \text{ nm}$)	2.6 km s $^{-1}$ (@ $t = 20 \text{ nm}$)
Freepath l	14.1 mm	22.5 μm	3.9 μm	9.3 μm	10.1 μm
Ratio l/λ	44.8	17.9	3.1	7.4	8.5
References	[8, 115–118]	[119–126]	[127–137]	[138–142]	[143–150]

2.2. Magnetic materials for magnonic applications

As was discussed in the previous section, spin waves are usually studied in thin magnetic films or waveguides fabricated in the form of narrow magnetic strips. The choice of magnetic material plays a crucial role in fundamental as well as applied magnonics. The main requirements are (i) a small-value Gilbert damping parameter α in order to ensure long spin-wave lifetimes; (ii) high saturation magnetization for high spin-wave frequencies and velocities; (iii) high Curie temperatures to provide thermostability; and (iv) simplicity in the fabrication of magnetic films and in the patterning processes.

The most commonly used materials for magnonics as well as those with a high potential for magnonic applications are presented in table 1 together with some selected parameters and estimated spin-wave characteristics. These characteristics are the spin-wave lifetime τ , defined by the Gilbert damping parameter α ; the spin-wave group velocity v , which, together with the lifetime, defines the spin-wave $1/e$ propagation distance (mean free path) $l = \tau v$; and the ratio of the mean free path to the wavelength l/λ . The latter is especially important for magnonic applications and its increase is one of the primary challenges facing the field [9]. Since practically all experimental studies in magnonics are performed nowadays for dipolar waves, the characteristics in the table are estimated using the dipolar approximation, where the exchange interaction is ignored. However, it has to be mentioned that the use of short-wavelength exchange waves appears to be promising, particularly with regard to the increase of l/λ .

The first material in the table is a monocrystalline $\text{Y}_3\text{Fe}_5\text{O}_{12}$ (YIG) film grown by high-temperature liquid-phase epitaxy (LPE) on gadolinium gallium garnet (GGG) substrates [115–118]. This ferrimagnet has the smallest known magnetic loss that results in a spin-wave lifetime of some hundreds of nanoseconds and, therefore, finds widespread use in academic research [8]. Most of the experimental results presented in this

thesis were obtained using LPE YIG. The small magnetic loss is due to the fact that YIG is a magnetic dielectric (ferrite) with very small spin–orbit interaction and, consequently, with small magnon–phonon coupling [118]. Moreover, the high quality of LPE single-crystal YIG films ensures a small number of inhomogeneities and, thus, suppresses two-magnon scatterings [13, 151]. However, the thickness of these films, which is in the micrometer range, does not allow for the fabrication of YIG structures of nanometer sizes. Therefore, the fabrication of nanostructures became possible only within the last few years with the development of technologies for the growth of high-quality nm-thick YIG films (see second column in table 1) by means of, e.g., pulsed-laser deposition [119–123], sputtering [124], or modification of the LPE growth technology [125, 126]. Although the quality of these films is still worse than that of micrometer-thick LPE YIG films, it is already good enough to satisfy many requirements of magnonic applications [9].

The second most commonly used material in magnonics is permalloy, which is a polycrystalline alloy of 80% Ni–20% Fe (see table 1). This is a soft magnetic material with low coercivity and anisotropies. One of the major advantages of this material is that it has a fairly low spin-wave damping value considering it is a metal, and it can be easily deposited and nanostructured [127–134]. Therefore, permalloy was intensively used for the investigation of spin-wave physics in microstructures (see reviews [135, 136]) and for investigations of magnonic crystals in particular [3, 5, 7, 134, 137]. Nowadays, considerable attention from the community is also focused on CoFeB [138–142] and half-metallic Heusler compounds [143–150]. These materials possess smaller Gilbert damping parameter values and larger values of saturation magnetization, and, therefore, are more suitable for the purposes of magnonics. For example, it was demonstrated that the spin-wave mean free path in Heusler compounds can reach 16.7 μm [149].

The fabrication of high-quality spin-wave waveguides is also one of the primary tasks in the field of magnonics. The most

Table 2. Techniques for excitation and detection of spin waves and their main features.

	Technique	Function	Features	References
Microwave techniques	Conventional microstrip antenna based approach	Excitation + detection	Coherent excitation, high sensitivity, phase control, high frequency resolution	[8, 130, 155, 156]
	Contactless antenna based approach	Excitation + detection	Simplified design without wiring, access to short-wavelength magnons	[157, 158]
	Ferromagnetic resonance (FMR) technique	Excitation + detection	Robust method for the characterization of magnetic materials	[128, 129, 159, 160]
	Parametric pumping technique	Amplification + excitation	Access to high magnon densities and short-wavelength magnons	[8, 22, 133, 161, 162]
	Pulsed inductive microwave magnetometer (PIMM)	Excitation + detection	Excitation of waves in a wide frequency range	[129, 163]
	Inductive magnetic probe (IMP) technique	Detection	Spatial resolution, high time and frequency resolution	[97, 164]
Optical techniques	Brillouin light scattering (BLS) spectroscopy	Detection	Space-, frequency-, time-, phase-, and wavenumber-resolved measurements	[3, 8, 134–136, 165–167]
	Thermal and nonthermal excitation by fs laser	Excitation	Access to high-frequency magnons, suitable for fundamental studies	[5, 168, 169]
	Magneto-optical Kerr effect (MOKE) spectrometry	Detection	Space, frequency, time, and phase resolutions	[157, 170]
Spintronic approaches	Spin pumping (SP) based technique detection	Detection	Direct conversion to DC, not sensitive to spin-wave wavelength	[9, 171–177]
	Spin transfer torque (STT) based technique	Amplification + excitation	Direct conversion from DC, efficient at nano-scale	[178–186]
	Spin-polarized electron energy loss spectroscopy (SPEELSC)	Detection	Access to high wavenumbers up to the edge of Brillouin zone	[187, 188]
Other techniques	Magneto-electric (ME) cells	Excitation + detection	Highly suitable for magnon logic	[189–191]
	Magnetic resonance force microscopy (MRFM)	Detection	High spatial resolution	[192]
	Detection of magnon-induced heat	Detection	Major opportunities for fundamental studies	[193]
	Nuclear resonant scattering	Detection	Highest spatial resolution currently achievable	[194]
	X-ray-detected ferromagnetic resonance (XFMR)	Detection	High spatial resolution, access to layer resolution	[195–197]
	Electron–magnon scattering approach	Detection	Suitable for the detection of domain wall position	[198, 199]

commonly used tool for the fabrication of micrometer-thick YIG waveguides in the form of magnetic strips is a dicing saw [152] since the width of the waveguide is usually greater than 1 mm. The main technique for the patterning of such YIG films is photolithography with subsequent wet etching by means of hot orthophosphoric acid [153]. At the same time the recently proposed laser-based patterning of YIG films shows large potential [154]. Another technique has been used to pattern nanometer-thick YIG films: e-beam lithography with subsequent Ar⁺ dry etching has shown good results [122, 125]. Focused ion beam milling has also recently shown very promising results—a 70 nm wide spin-wave waveguide was fabricated into a 100 nm thick YIG film at the Nano Structuring Center at the University of Kaiserslautern (not published). The same techniques can also be used for the patterning of metallic magnetic films. However, a different approach is often used: The magnetic material is

deposited on a resist mask produced via photolithography or electron beam lithography followed by a standard lift-off process. Antennas and the required contact pads are deposited afterward in subsequent lithography and lift-off processes.

2.3. Methods of spin-wave excitation and detection

Modern magnonics consists of a wide range of instrumentation for the excitation and detection of magnons. The most commonly used techniques as well as techniques showing huge potential are given in table 2 with references and brief descriptions of their particular features. It can be seen that the three main categories are microwave, optical, and spintronic approaches. The main requirements for magnon detection techniques could be defined as sensitivity, the range of detectable wavelengths and frequencies, and frequency, spatial,

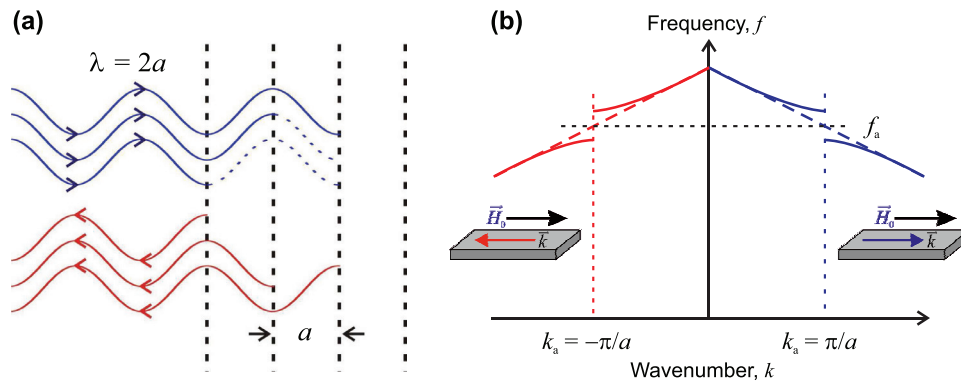


Figure 3. (a) Sketch of Bragg reflection of a spin wave having an incident angle $\theta = \pi/2$ from a one-dimensional magnonic crystal. The Bragg law for the particular case shown in the figure is defined. (b) Schematic of the BVMSW modes' dispersion curves in a uniform magnetic film (dashed lines) and in a magnonic crystal (solid lines). The formation of a band gap at the frequency corresponding to a spin-wave wavenumber of $\pm\pi/a$ is shown.

and temporal resolution. For spin-wave excitation techniques the efficiency of excitation, its coherency and the wavenumber range are of primary importance [155–157, 159, 160, 163–165, 168–172, 174, 177–189, 191–199].

The conventional technique for spin-wave excitation is inductive spin-wave excitation with a microwave current sent through a strip-line antenna. In order to understand the spin-wave signal excitation mechanism, it is useful to consider the waveguide as a reservoir of quasi-classical spins. When the waveguide is magnetically saturated, the mean precessional axis of all the spins is parallel to the bias field. Application of a microwave signal to the strip-line antenna generates an alternating Oersted magnetic field around it. Components of this field which are perpendicular to the bias direction create a torque on the magnetization, which results in an increase in the precessional amplitude [8, 155, 156]. Spins that precess under the antenna interact with their nearest neighbors. If the correct conditions for the field and frequency are satisfied, spin-wave propagation is supported. After propagation, the spin-wave excitation might be detected by a similar output antenna. The mechanism of spin-wave detection is, by symmetry, the inverse of the excitation process.

The most popular of the other detection techniques in magnonics nowadays is probably BLS spectroscopy [8, 135, 136, 165]. The physical basis of BLS spectroscopy is the inelastic scattering of photons by magnons. Scattered light from a probe beam incident on the sample is analyzed, allowing the frequencies and wavenumbers of the scattering magnons to be determined, where the scattered photon intensity is proportional to the spin-wave intensity. The technique is generally used in conjunction with a microwave excitation scheme and, over the last decade, has undergone extensive improvements. BLS spectroscopy now achieves a spatial resolution of 250 nm, and time-, phase-, and wavenumber-resolved BLS spectroscopy has been realized [3, 8, 134–136, 165–167].

3. Static magnonic crystals

3.1. Spin-wave Bragg scattering conditions in magnonic crystals

Magnonic crystals, whose name refers to the spin-wave quasiparticles magnons, are artificial magnetic media whose

magnetic properties are characterized by periodic variation in space [28]. Similar to photonic crystals operating with light, magnonic crystals use the wave nature of magnons to obtain magnon propagation characteristics that are inaccessible by any other means (see reviews [3–9]). Bragg scattering affects a spin-wave spectrum in such a periodic structure and leads to the formation of band gaps—frequencies at which spin-wave propagation is prohibited.

Figure 3(a) shows schematically the mechanism of Bragg scattering in a one-dimensional magnonic crystal in the form of a periodic array of reflectors with a lattice constant a . The incident spin-wave angle θ in this case is equal to $\pi/2$. In most of the experiments, the reflection efficiency of the wave from a single reflector is rather low and varies from 1% to 10% [134, 137, 153] while the number of reflectors is usually limited to 20 due to a relatively large spin-wave loss [8]. In such a situation, the majority of the spin-wave energy propagates through the crystal with small parasitic loss if the Bragg condition $n\lambda = 2a \cdot \sin \theta$ is not satisfied (n is an integer value). In contrast, when the Bragg condition is satisfied, as shown in the figure, the spin waves that are reflected from each dashed line have the same phase providing a resonant reflection condition. The major part of the energy of such a spin wave will be reflected from the magnonic crystal. The dashed lines in figure 3(b) show simplified linearized dispersion curves for BVMSW modes propagating in an infinitely extended film along the biasing magnetic field in both directions. If the spin wave propagates through a magnonic crystal, waves with wavenumber $k_a = \pm n\pi/a$ satisfying the Bragg condition are reflected, resulting in the formation of a band gap at the frequency f_a (for $n = 1$) as schematically shown in the figure. The width of the band gap is usually defined by the reflection efficiency of a single reflector [105].

As mentioned previously, spin-wave properties can be tuned by a variety of different parameters, such as the thickness of the magnetic film, the width of the spin-wave waveguide, the saturation magnetization of the magnetic material and the applied biasing magnetic field [13, 14]. This opens up many possibilities for the realization of magnonic crystals, since each of these parameters can be varied periodically in space. If the parameters are constant over time (e.g. they are defined only by the sample geometry), these magnonic

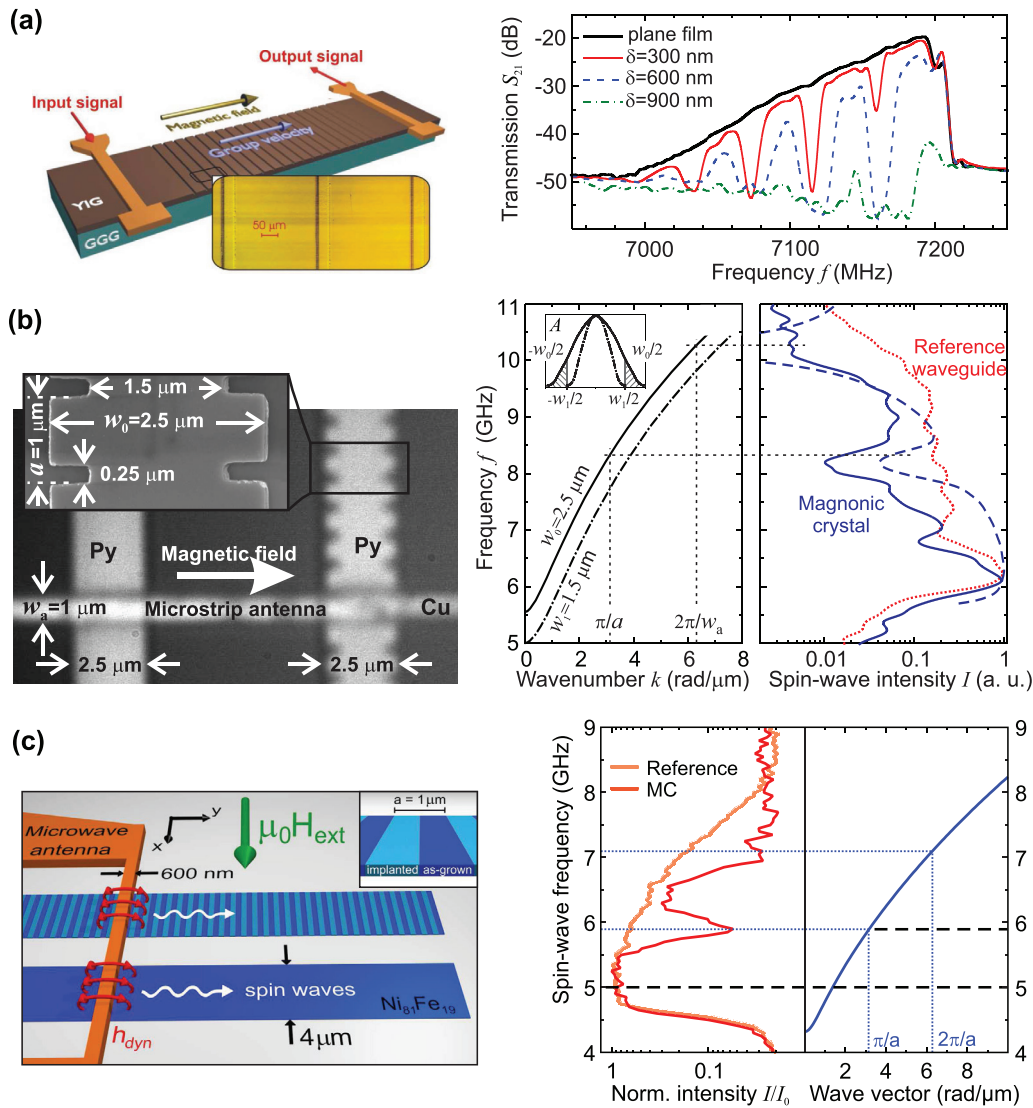


Figure 4. Different realizations of static magnonic crystals. (a) Sketch of a magnonic crystal structure comprising an array of shallow grooves on the surface of a YIG film. The BVMSW transmission characteristics for magnonic crystals for different groove depths δ are shown [153]. (b) Scanning electron microscopy and optical images of a width-modulated micro-scaled magnonic crystal together with a reference unpatterned waveguide. The calculated spin-wave dispersion curves and measured spin-wave intensity for the magnonic crystal and reference waveguide are shown on the right [134]. (c) Schematic of the experimental setup for studies of micro-structured ion-implanted magnonic crystal [137]. Normalized spin-wave transmission spectra of the magnonic crystal waveguide (red line) and the reference waveguide (amber line) as well as the calculated spin-wave dispersion curves are shown on the right.

crystals are termed static. The schematics of different types of static one-dimensional magnonic crystals together with their measured characteristics are shown in figure 4.

3.2. YIG magnonic crystals based on the periodic variation of film thickness

Geometric structuring of a uniform spin-wave waveguide by fabricating an array of grooves on its surface is a simple and highly efficient means of magnonic crystal fabrication [1, 29, 153, 200, 201] (see figure 4(a)). Photolithographic patterning followed by hot orthophosphoric acid etching (this etching technology utilizing the procedure of ultraviolet hardening of resist was developed at the Nano-Structuring Center of the University of Kaiserslautern [153, 200]) has been shown to be a reliable means of forming the required grooves in a YIG

spin-wave waveguide. The spectra of transmitted spin waves in such structures have been studied experimentally and theoretically for BVMSWs [153] (see right panel in figure 4(a)) and surface magnetostatic waves [200]. Special attention has been paid to the study of magnonic crystal microwave characteristics as a function of groove depth [153, 200, 201]. Pronounced rejection frequency bands have been clearly observed (more than 30 dB rejection was achieved) and it was shown that the rejection efficiency and the frequency width of the rejection bands increase with increasing groove depth (right panel in figure 4(a)). In addition, it has been found that the rejection of the BVMSW mode is considerably (up to 600 times) greater than that of the MSSW modes. This is related to the nonreciprocal nature of the MSSW mode as well as to the resonant scattering of the lowest BVMSW mode into higher thickness modes [200].

Detailed studies of this magnonic crystal and its optimization have been performed in [201]. It was shown that the efficiency of rejection can be controlled not only by the groove depth, but also by the groove width and by the number of grooves in the crystal. When the width of grooves is much smaller than the spin-wave wavelength, increasing the groove width leads to a rapid increase in rejection efficiency. The efficiency of rejection also increases with an increase in the number of grooves. It was further found that the optimal groove depth, which ensures strong rejection in the rejection bands while maintaining a low insertion loss of around 3 dB in the transmission bands, is approximately 1/10 of the total film thickness for the BVMSW mode. Decreasing the groove depth further leads to an increase in rejection efficiency in the band gap regions as well as in an increase in parasitic loss in the transmission bands [201].

A theoretical model was developed to describe spin-wave transmission through a magnonic crystal [153]. The model is based on the introduction of transmission T-matrices for spin waves at spatial points where the thickness of the YIG waveguide changes (steps), as well as for sections of the waveguide with constant thicknesses [201]. As a result, the T-matrix for each periodic segment of a magnonic crystal was found as a multiplication of four different matrices, two for the steps and two for the sections in between. In order to obtain the transmission characteristics for the whole magnonic crystal, this matrix was raised to the power equal to the number of periods. The results of this simple theoretical model have shown good qualitative agreement with the experimental results. Subsequently, this model was adopted to describe magnonic crystals with smooth transformations in magnetic properties [202].

3.3. Micro-structured metallic magnonic crystals based on the periodic variation of the spin-wave waveguide width

The groove-based magnonic crystals discussed above have macroscopic sizes (a typical lattice constant is 300 μm). Modern signal-processing applications, however, demand magnonic crystals of sub-micron sizes. The nano-scaled magnonic crystal proposed in [203] has been fabricated from a permalloy waveguide by engineering periodic variations in its width (see figure 4(b)) [134]. This system was studied experimentally using micro-focused Brillouin light scattering spectroscopy. A spin-wave band gap was clearly observed (see right panel in figure 4(b)). It is seen as a considerable decrease in the spin-wave transmission caused by resonant backscattering from the periodic structure. The band gap frequency was tuned in the range of 6.5 to 9 GHz by varying the applied magnetic field. The results presented in [134] are the first experimental realization of spin-wave propagation through a micro-structured magnonic crystal. The spin waves were excited here by a microstrip antenna deposited onto the top of the permalloy waveguide. Another interesting method of magnon injection to width-modulated magnonic crystals from a semi-infinite magnetic film was proposed and experimentally verified in [204].

The transmission characteristics of permalloy-based width-modulated crystals were also investigated by numerical

simulations [205, 206]. The magnonic crystal was represented by a micro-sized planar ferromagnetic waveguide with periodically changing width. By choosing a step-like or sinusoidal variation of the width, the magnonic crystal revealed multiple or single band gaps, respectively [205]. In addition, it was found that both the band gap frequency and depth depend strongly on the probing position inside the magnonic crystal due to the non-uniform distribution of the internal magnetic field. The dependence of the spin-wave spectrum on the position inside the magnonic crystal was also studied in [207].

3.4. Micro-structured metallic magnonic crystals based on the periodic variation of the saturation magnetization

A micromagnetic analysis of spin-wave propagation was performed for a magnonic crystal realized as a permalloy spin-wave waveguide with a periodical spatial variation of its saturation magnetization [208]. Frequency band gaps were clearly observed in the spin-wave transmission spectra, and their origin was traced back to an overlap of individual band gaps of the fundamental and higher-order spin-wave width modes. This superposition could be controlled by the width of the magnonic crystal waveguide. Furthermore, the depths of the rejection bands depend strongly on both the level of the magnetization variation and the size of the area with a reduced magnetization: The reduction of saturation magnetization over a larger area leads to the formation of more pronounced band gaps.

As a proof of concept, a micro-structured permalloy-based magnonic crystal was fabricated by localized ion implantation (see figure 4(c)) and was investigated in comparison with a reference permalloy waveguide by means of Brillouin light scattering microscopy [137]. The irradiation caused a periodic variation in the saturation magnetization along the waveguide. It has been found that a slight modification of the saturation magnetization by 7% is sufficient to decrease the spin-wave transmission in the band gaps by a factor of 10 (see right panel in figure 4(c)). Since the waveguide consisted of a single, topographically unchanged material, spin waves with frequencies in the transmission bands were nearly unaffected. These results prove the applicability of localized ion implantation for the fabrication of efficient micron- and nano-sized magnonic crystals for magnon spintronic applications.

4. Reconfigurable, dynamic, and moving magnonic crystals

Reconfigurable magnonic crystals, whose properties can be changed on demand [7, 209–216], attract special attention since they allow for tuning of the functionality of a magnetic element: the same element can be used in applications as a magnon conduit, a logic gate, or a data-buffering element. An example of such a structure is a magnonic crystal in the form of an array of magnetic strips magnetized parallel or anti-parallel to one another [209]. The chosen magnetization state defines the lattice constant of the crystal and, thus, the spin-wave dispersion.

From the point of view of low energy consumption, voltage-controlled reconfigurable magnonic crystals are of particular

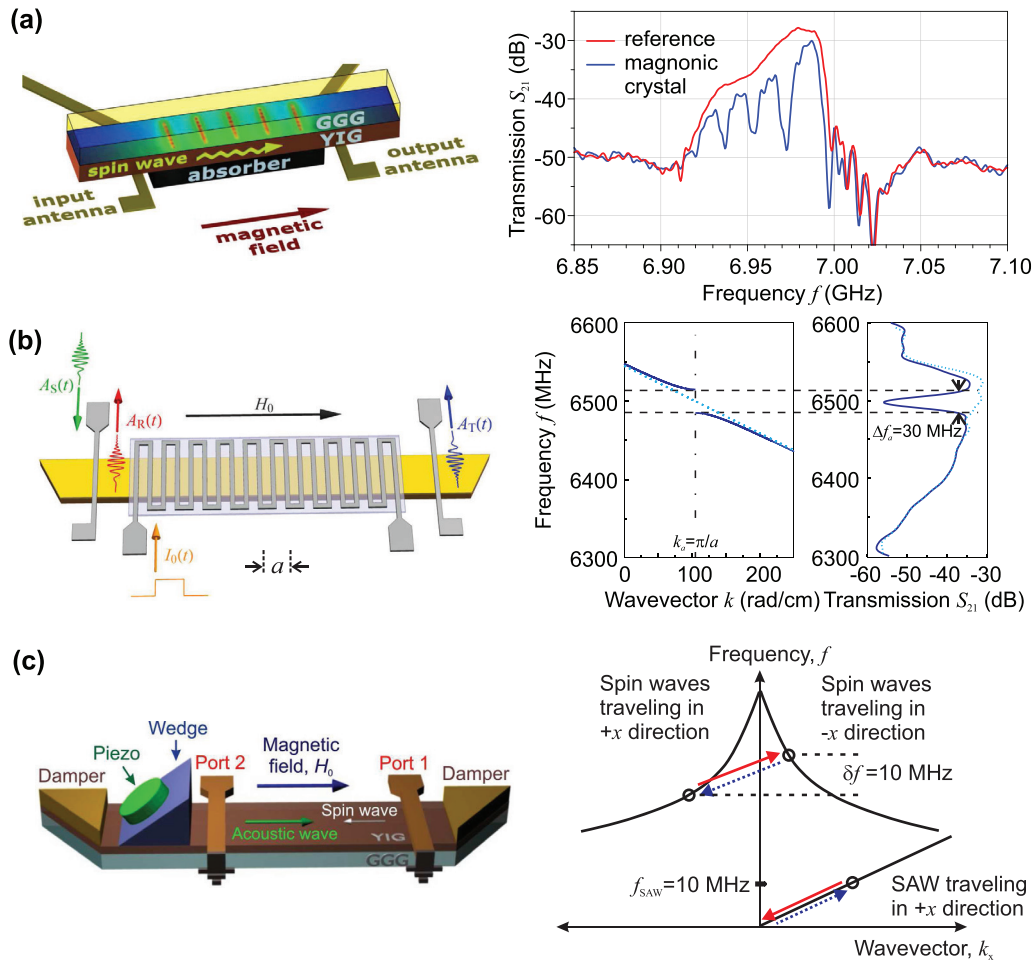


Figure 5. Reconfigurable (a), dynamic (b), and traveling (c) magnonic crystals. (a) Schematic of the reconfigurable magnonic crystal with a GGG/YIG/absorber multilayer system [202]. A typical thermal landscape is shown on the waveguide (color code: red, maximum temperature; blue, minimum temperature). Right panel: Measured spin-wave transmission characteristic (solid blue line) in the thermal landscape (magnonic crystal with five periods, lattice constant $740 \mu\text{m}$) and reference data (red) without the projected pattern. (b) Schematic of the dynamic magnonic crystal comprising a planar current-carrying meander structure with 20 periods with a lattice constant $a = 300 \mu\text{m}$ (10 shown), positioned close to the surface of the YIG spin-wave waveguide. Right panel: Dispersion characteristic and measured spin-wave transmission characteristic of this dynamic magnonic crystal for 1 A current sent through the meander structure [219]. (c) Schematic of the moving magnonic crystal. The spin waves are excited and detected in the YIG film by stripline antennas. The surface acoustic wave is excited on the YIG/GGG sample by a piezoelectric quartz crystal and an acrylic wedge transducer [221]. Right panel: Schematic of the dispersion curves for the BVMSW and SAW. Circles indicate waves that participate in Bragg scattering.

interest. A nano-scale reconfigurable magnonic crystal designed using voltage-controlled perpendicular magnetic anisotropy (PMA) in ferromagnetic-dielectric hetero-structures was investigated using numerical simulations in [217]. A periodic array of gate metallic stripes was placed on top of a MgO/Co structure in order to apply a periodic electric field and to modify the PMA in the Co. It is demonstrated that the introduction of PMA modifies the spin-wave propagation and leads to the formation of band gaps in the spin-wave spectrum. The band gaps' characteristics are defined by the applied electric field and can be controlled dynamically, i.e. it is possible to switch the band gaps ON and OFF within a few tens of nanoseconds.

4.1. Optically induced reconfigurable magnonic crystals

An important step toward the realization and study of reconfigurable magnonic crystals was the demonstration that any two-dimensional magnetization pattern in a magnetic film

can be created in a reconfigurable fashion by laser-induced heating [202]. By using a laser, a thermal landscape in a magnetic medium was created (see figure 5(a)) that resulted in an equivalent landscape of the saturation magnetization [218] and, hence, in the control of the spatial spin-wave characteristics. The setup used for the realization of the light patterns consisted of a continuous-wave laser as a light source, an acousto-optical modulator for temporal intensity control, and a spatial light modulator for spatial intensity control. In order to study the influence of the thermal gradient induced by the intensity patterns on the spin waves, we used a ferrimagnetic, $5 \mu\text{m}$ thick YIG waveguide grown on a $500 \mu\text{m}$ thick GGG substrate (see figure 5(a)). GGG is almost transparent, while YIG absorbed about 40% of the green light used in the experiment. In order to increase the efficiency of the heating, we used a black absorber coated on top of the YIG film. The proposed concept of a reconfigurable magnetic material was demonstrated and tested on the example of one- and

two-dimensional magnonic crystals. The formation of band gaps in the spin-wave transmission characteristic is shown in the right panel of figure 5(a). It was demonstrated that the positions of the band gaps can be tuned by the lattice constant of the magnonic crystal, while the widths of the band gaps were controlled by the laser light intensity [202].

4.2. Current-controlled dynamic magnonic crystals

Changes in the properties of a magnonic crystal open up access to novel physics if these changes occur on a timescale shorter than the time of spin-wave propagation through the crystal. Such magnonic crystals are termed dynamic magnonic crystals [10, 219]. The first dynamic magnonic crystal was realized by employing a YIG waveguide placed in a spatially periodic dynamically controllable magnetic field provided by a current-carrying planar metallic meander structure (figure 5(b)) [219]. The current-carrying structure was spaced at a distance of 100 μm above the YIG surface in order to avoid undesirable interaction between the spin waves and the conductor [220]. Since the lateral variations of the bias magnetic field were approximately sinusoidal inside of the YIG film, the spectrum of the crystal contained only one space component and a sole rejection band appeared (see right panel in figure 5(b)). It was demonstrated that the rejection band depth and width could be tuned via the applied current [10, 219]. Furthermore, it was shown that such a crystal could be switched from a full transmission to a full rejection state faster than 10 ns, which is a tenth of the spin-wave relaxation time and the time of spin-wave propagation through the crystal. The possibility of achieving fast temporal variation of crystal parameters opened doors to the study of new physical effects, as discussed in the following section.

Another approach for the realization of a dynamic magnonic crystal was proposed in [110], based on the control of the effective geometry of a magnetic film waveguide for spin waves via electric current. The device utilizes a spin-wave waveguide fabricated from a YIG waveguide of periodically varied width and two conducting wires attached to the film surface along the modulated edges. A spatially uniform bias magnetic field is directed across the YIG waveguide. Positive currents applied to both wires induce an additional negative Oersted field that reduces the bias magnetic field near the edges. The magnetic wells which are thus created screen the YIG film's modulated edges from spin waves and, hence, suppress the magnonic crystal band gap. The advantages of the width-modulated dynamic magnonic crystal over those utilizing meander wiring [219] are potentially fast performance and possibility for miniaturization. Indeed, current control is provided here by short conductors, which have an inductance much lower than that of the meander-type wire. The use of nanostructured width-modulated waveguides made of permalloy films (figure 4(b)), as in [134], will allow for a significant reduction of the magnonic crystal size. This type of dynamic magnonic crystal has been used to perform AND logic gate operation [110].

4.3. Surface acoustic wave based moving magnonic crystals

Moving magnonic crystals represent a special class of dynamic and tunable crystals utilizing moving Bragg gratings. Such magnonic crystals have been created via a periodic strain induced by a surface acoustic wave (SAW) traveling along a YIG spin-wave waveguide as shown in figure 5(c) [100, 221–223]. Spin-wave scattering in such a crystal differs conceptually from the previously discussed cases since it takes place with a shift in the spin-wave frequency due to the Doppler effect. In fact, a combination of Bragg scattering with the Doppler shift took place in the experiments [221]. The schematic of such scattering is shown in the right panel of figure 5(c). One can see that in order to fulfill the conservation laws, the magnon scattering should occur with a shift in the frequency equal to the frequency of the SAW. The wavelengths of the spin waves and SAW should be comparable in order to satisfy momentum conservation.

The experiment was performed using BVMSWs characterized by negative group velocity [111]. As a result, spin waves scattered from an approaching grating were found to be shifted down in frequency, demonstrating the reverse Doppler effect [221]. In contrast to [224], here the reflection occurred from a crystal lattice rather than from a single reflecting surface and, thus, the wavenumber of the scattered wave was strictly determined by the law of conservation of momentum. Due to this fact, the frequency-shifted wave appeared as a single narrow peak in the transmission characteristic of the magnonic crystal. Apart from such interesting physics, these systems show potential for sensors and signal-processing applications.

5. Magnonic crystal based data processing

5.1. Magnonic crystal as a microwave filter

One of the initial motivations in the study of spin-wave propagation through periodic magnetic structures was the realization of microwave filters and resonators for the processing of analog information—see review [1]. The magnonic crystals described above can also be used for these purposes. One can see in the spin-wave transmission characteristics shown in figures 4 and 5 that the spin-wave spectra of a magnonic crystal comprise regions of frequencies for which the transmission of microwave signals is prohibited. Thus, a magnonic crystal can serve as a stop-band filter. The attenuation of the microwave signal in the stop band exceeded 30 dB in our experiments [153], but was limited by the experimental conditions. Theoretical modeling has shown that this value might actually be much greater and can exceed 100 dB.

The advantage of such filters is that the central frequencies of the stop bands can easily be controlled by an applied magnetic field [134, 137] or by the lattice constant of the magnonic crystal [202]. The width of the band gap, which is usually close to several tens of MHz, is defined by the strength of the modulation of a magnetic property (e.g. groove depth [153], magnetic field [219], saturation magnetization [137], mechanical stress [221] or temperature [202]) or by the

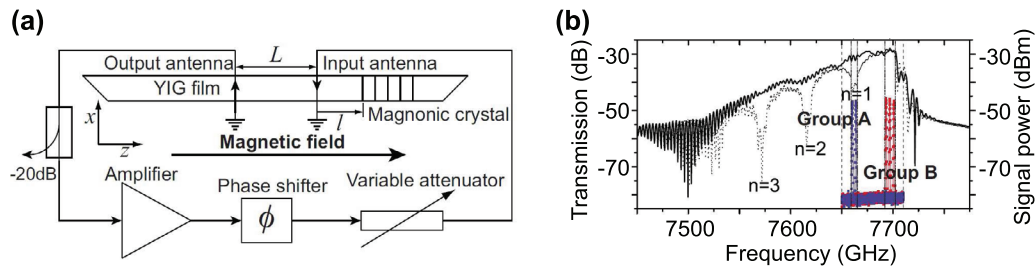


Figure 6. (a) Schematic of an experimental active ring system employing a magnonic crystal to define the wavenumber of the resonance mode. Two microstrip antennas excite and receive spin waves through a region of the YIG film. A magnonic crystal, which is part of the same film, is located in close proximity to the input antenna. (b) BVMSW transmission characteristics for the uniform (bold, solid) and magnonic crystal (dotted) regions of the YIG film (left ordinate axis). The inset diagram (right ordinate axis) is a composite of five overlaid ring power spectra for different distances between the input antenna and the magnonic crystal [102].

thickness of the magnetic film that defines the slope of the spin-wave dispersion [201]. The number of band gaps in spin-wave spectra is given by the variation function of the magnetic properties [205] (step-like functions result in multiple band gaps [153]; harmonic variation of properties results in a single band gap [219]). Moreover, one of the greatest advantages of such filters is determined by the fact that the spin-wave wavelengths are orders of magnitude smaller than the wavelengths of electromagnetic waves in the same GHz frequency range. That allows for a considerable miniaturization of the devices (e.g. magnonic crystals of micrometer sizes have been realized [134, 137]). Finally, reconfigurable and dynamic magnonic crystals allow for the realization of microwave filters that can be tuned or switched ON/OFF on a nanosecond time-scale [219].

On the other hand, the main drawbacks of microwave filters based on magnonic crystals are probably the relatively low efficiencies of spin-wave excitation and detection by standard micro-strip antennas and the relatively high values of spin-wave damping. This induces loss in the transmission bands of the filter, which, in our experimental demonstrations, usually exceeds 10 dB (see figures 4 and 5). By utilizing thicker magnetic films and optimized microwave antennas, this value can be improved but will probably still be close to a few dB [1, 2].

5.2. Microwave signal generation based on magnonic crystals with a feedback loop

The spin-wave systems discussed above also allow the realization of coherent microwave sources. Self-exciting positive-feedback spin-wave systems, often termed spin-wave active rings, are used for this purpose [225, 226]. The basis for such an active ring is a dispersive spin-wave waveguide with exciting and receiving antennas connected together via a variable-gain electrical feedback loop (see figure 6(a)). If the correct gain and phase conditions are met, a monochromatic (but noise-initiated) signal propagates in the ring, and increases with time until nonlinear saturation takes place either in the spin-wave system or in the external amplifier. The signal from the active ring can be partially extracted using a directional coupler as shown in the schematic.

Spontaneous excitation of an active ring system occurs if the external gain is increased beyond the self-generation threshold of the spin-wave mode with the smallest threshold. This mode

is called the dominant mode and suppresses the excitation of all other modes in the quasi-linear regime. However, the wavenumber of this dominant mode, which defines the generated frequency, is highly sensitive to the internal magnetic field and the thermal environment of the spin-wave transmission medium. As a result, in any real system it is almost impossible to predict the wavenumber of the dominant mode. It was demonstrated, however, that exploitation of spin-wave reflections from a groove-based magnonic crystal allows for the selection of the wavenumber of the dominant mode [102].

The active ring shown in figure 6(a) operates with BVMSWs that are reciprocal. This means that spin waves excited by the input antenna propagate in both directions of the waveguide. In order to achieve an auto-oscillation regime of the ring, constructive interference between the signal detected at the output antenna, amplified and fed back to the input antenna, and the signal reflected from the magnonic crystal (see schematic) is required. The tuning of the phases of both signals plays a crucial role in this case. The phase of the signal from the output antenna is tuned by the external phase shifter, while the phase of the signal reflected from the magnonic crystal is defined by the distance between the input antenna and the first groove of the crystal. Thus, by changing the position of the crystal relative to the antennas, different dominant modes were excited in the experiment (see figure 6(b)). Excitation of two different groups of modes was observed. Group B corresponds to the conventional operating regime of the active ring, in which the magnonic crystal does not play any role. It occurred at frequencies where the spin-wave transmission was close to its maximum. In contrast, the wavenumbers of the spin waves of group A were determined by the magnonic crystal characteristics and lay within the first band gap. The position of the magnonic crystal relative to the antennas defined which of the three modes inside the band gap were generated. Thus, when the mode enhancement phase conditions were satisfied, the ring geometry permitted highly robust forced dominant wavenumber selection [102].

Furthermore, it was demonstrated in [103] that a delay line based on a one-dimensional magnonic crystal used in the feedback loop of a microwave auto-oscillator can substantially reduce the phase noise figure and improve other vital performance characteristics of the auto-oscillator. It is also interesting that the frequency selectivity of a magnonic crystal with a quasiperiodic Fibonacci-type structure may provide

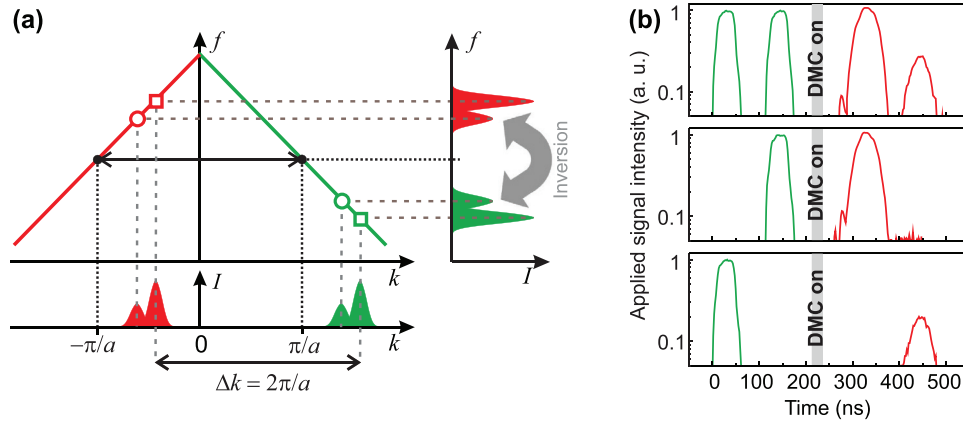


Figure 7. Frequency inversion and time reversal by a dynamic magnonic crystal [104]. (a) Schematic of the frequency inversion process. (b) The experimentally detected spin-wave signals reflected by the dynamic magnonic crystal. The gray area shows the time during which the dynamic magnonic crystal was switched ON.

conditions for the self-generation of dissipative solitons in an active spin-wave ring [49, 51].

5.3. Frequency inversion and time reversal using dynamic magnonic crystals

In the previous section, we discuss the transmission properties of our proof-of-concept dynamic magnonic crystal when it is kept in either the OFF or the ON state (see figure 5(b)). In follow-up studies, it was demonstrated that dynamic magnonic crystals open up access to new physical effects if the crystal is switched from OFF to ON while a spin-wave packet is inside [104, 105].

If a spin wave with wavevector $k_s \approx +k_a = +\pi/a$ is incident on the dynamic magnonic crystal while it is in the ON state, it is reflected with conservation of the frequency. However, if the crystal is switched from OFF to ON while such a wave is inside, the situation is quite different [104]. In figure 7(a) the dispersion curves for incident signal waves (green section) and those reflected by the magnonic crystal (red section) are shown. Black dots mark the reference frequency f_a lying in the center of the band gap and corresponding to the Bragg wavevectors $\pm k_a = \pm\pi/a$. The green open circle and square illustrate two spectral components of the incident signal waveform. The spatially periodic magnetic modulation of the waveguide’s magnetic bias field, brought about by the application of the current pulse to the dynamic magnonic crystal meander structure (see figure 5(b)), couples these components to corresponding components of the reflected waveform (red open circle and square). The difference between the wavevectors of the signal and reflected waves is fixed by the lattice constant a of the dynamic magnonic crystal such that the k -spectrum of the reflected waveform is uniformly shifted to the left by $\Delta k = 2\pi/a$ (lower panel). This shift results in a spectral inversion in the frequency domain. The frequency inversion in a range of frequencies of ± 15 MHz has been shown experimentally [10, 104, 105].

Time-reversing a signal is equivalent to inverting its spectrum about a reference frequency. This can be easily proven by considering the Fourier domain description of an arbitrary signal envelope which shows that the frequency inversion is

equivalent to the transformation $t \rightarrow -t$. In order to demonstrate the spin-wave time reversal a BVMSW packet consisting of two pulses was used—see figure 7(b). Switching OFF of the first or the second pulse has clearly demonstrated that the spin-wave packet reflected by the magnonic crystal is reversed in time: When two spin-wave pulses are applied, two corresponding pulses reflected by the dynamic magnonic crystal are observed (upper frame, red). When the first of the two pulses is switched OFF, the second reflected pulse is absent (middle frame), and vice versa (lower frame), confirming time reversal [104].

Thus, it was shown that a dynamic magnonic crystal may provide a linear means to perform spectral transformations, including frequency inversion and time reversal, which, until now, have only been possible through nonlinear mechanisms [20, 21, 227, 228]. These results go far beyond spin waves since they can be applied to waves of any nature. For example, the idea of all-linear time reversal was taken up by Sivan and Pendry in the field of photonics [229].

5.4. Data buffering in standing magnonic crystal modes

The deceleration or even full stop of light due to the modification of the light dispersion in photonic crystals has been a topic of intensive studies over the last decade [230, 231]. A wave of light propagating through a photonic crystal is coupled with the internal standing crystal mode and generates a slow light mode which can be used for storage of optical signals. Magnonic crystals as the magnetic counterpart of photonic crystals operate with spin waves and can demonstrate similar effects in the GHz frequency range. However, in spite of the progress in magnonic crystal studies, no significant spin-wave deceleration has been demonstrated. This is due to pronounced spin-wave damping, which limits the maximum number of structure periods to 20 or so. The small number of periods implies that the group velocity of spin waves, rather than vanishing, only slightly decreases at the gap edges [106]. Experimental investigations of groove-based magnonic crystals have shown that the spin-wave velocity can be decreased by about 20 percent at the edges of band gaps [106].

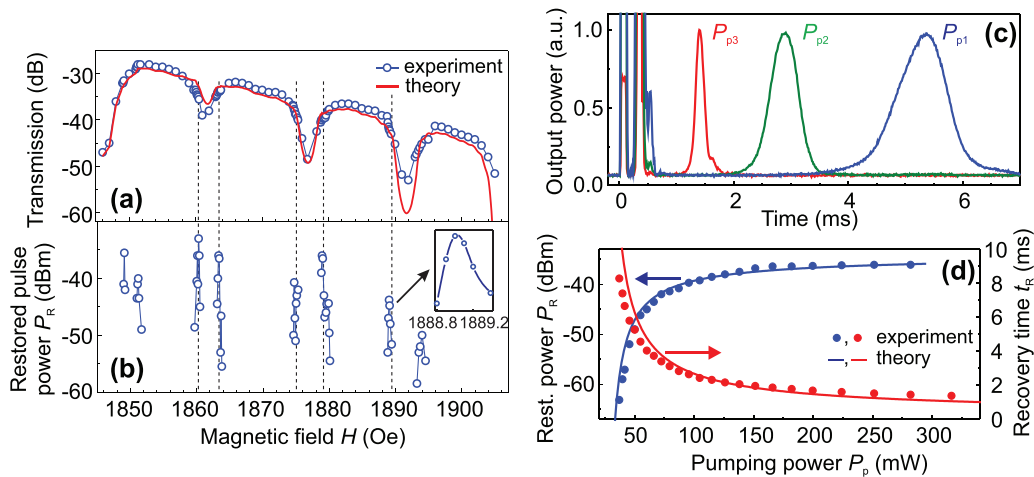


Figure 8. Microwave signal restoration in a parametrically driven magnonic crystal [106]. (a) Transmission of the spin-wave signal as a function of the bias magnetic field. (b) Power of the restored pulse as a function of the field. One sees that the restored signal is visible only at the edges of the band gaps. (c) Time profiles of the restored signal measured at a 1860 Oe magnetic field for different pumping powers: $P_{p1} = 50$ mW, $P_{p2} = 90$ mW, $P_{p3} = 320$ mW. (d) Measured (circles) and calculated (lines) dependencies of the restored signal power and recovery time as a function of the pumping power.

Nevertheless, it was demonstrated that storage of spin information in spin-wave modes is also possible in magnonic crystals. Unlike the conventional scheme used in photonics, this trapping occurs not due to the deceleration of the incident wave when it enters the periodic structure [230, 231] but due to the excitation of quasi-normal modes of an artificial crystal [106]. The first quasi-normal mode, whose eigenfrequency coincides with the minima of the spin-wave group velocity at the edges of the magnonic crystal's band gaps, has the longest lifetime among all the modes and, thus, conserves the signal energy and phase information for a long time after the propagating wave has left the magnonic crystal. Such a trapped spin-wave signal can subsequently be restored to its traveling form by means of double-frequency parametric amplification. One can see in figures 8(c) and (b) that the restoration and, thus, the storage occur only at the edges of the magnonic crystal band gap [106].

Figure 8(c) shows the time profiles of the restored signals for different pumping powers. The amplitude, the time of appearance and the duration of the restored signal were determined by the pumping power. The restoration mechanism based on a competitive nonlinear amplification process has been proposed earlier [232] and a corresponding theoretical model has been developed [233] for the case of featureless thin magnetic films. This model describes the dependencies of the restored pulse amplitude, duration, and delay as a function of pumping power with high accuracy (see solid lines in figure 8(d)). The longest delay between the excitation of the data-carrying spin-wave pulse, which propagated through the magnonic crystal, and the application of the pumping pulse to read out this information was $1.6 \mu\text{m}$ in the experiments [106]. Thus, the proposed physical phenomena can be used for short-time data buffering, over a few microseconds, but not for long-time storage.

In addition, investigations of parametric interactions between spin waves and electromagnetic pumping in magnonic crystals have yielded extremely interesting insight

into nonlinear wave physics. In such systems, parametrically coupled waves propagating in opposite directions are simultaneously coupled by the Bragg reflection law. As a result, parametric instability in magnonic crystals exhibits a strongly phase-dependent behavior [106].

5.5. Magnonic crystals in spin-wave logic devices

One of the strengths of magnonics lies in the benefits provided by the wave nature of magnons for the processing of digital data and computation. Nowadays, new technologies, allowing for example the fabrication of nanometer-sized structures or operation in the THz frequency range, in combination with novel physical phenomena, provide new momentum to the field and make magnonic crystals especially promising for controlling and manipulating magnon currents [9]. The idea of encoding binary data into the spin-wave amplitude was first proposed in a theoretical study [234] and the first experimental steps in this direction were made in [235]. It was proposed to use a Mach-Zehnder spin-wave interferometer equipped with current-controlled phase shifters embedded in the interferometer arms to construct logic gates. Following this idea, proof-of-principle XNOR and NAND logic gates were realized shortly thereafter [236].

The dynamic magnonic crystal based on a width-modulated waveguide [110] discussed above can also be used as a logic gate. The operating principle is based on controlling the bias magnetic field distribution along the sinusoidal borders of the YIG film waveguide through a change in the electric currents I_1 and I_2 . Logic '0' represents zero input current and logic '1' the current which is enough to 'switch OFF' the width modulation on one side of the magnonic crystal. The microwave pulses at the input antenna represent clock pulses. The microwave signal at the output antenna serves as the logic signal output. The operational frequency of the device corresponds to the central frequency of the band gap. Therefore, the presence of a band gap (i.e. a low power level at the output)

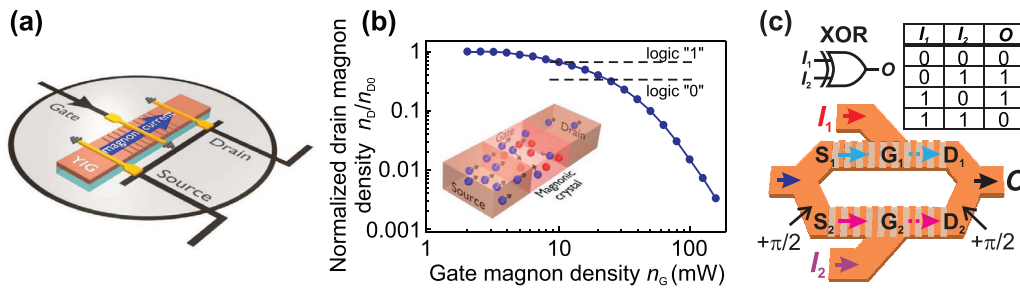


Figure 9. (a) Schematic of the magnon transistor [108]. The transistor is based on a magnonic crystal designed in the form of a YIG film with an array of parallel grooves on its surface. The magnons are injected into the transistor’s source and are detected at its drain using microstrip antennas. (b) The measured drain magnon density is presented as a function of the gate magnon density. The horizontal dashed lines define the drain density levels corresponding to logic ‘1’ and logic ‘0’. A schematic of the operational principle of a magnon transistor is shown in the inset. The source-to-drain magnon current (shown as blue spheres) is nonlinearly scattered by gate magnons (red spheres) injected into the gate region. (c) Magnon-crystal-based all-magnon chip proposed for XOR logic operation and the corresponding truth table.

is represented by logic ‘0’ and the absence of a band gap is represented by logic ‘1’. It is proven experimentally that logic ‘0’ appears at the output port in three situations: for two logic ‘0’ applied to the input ports and for combinations of logic ‘0’ and logic ‘1’ applied to the inputs. In the case where logic ‘1’ is applied simultaneously to both inputs, the band gap disappears, the spin wave passes through the magnonic crystal, and the signal at the output port corresponds to logic ‘1’. Thus, the performance of the dynamic magnonic crystal as an AND logic gate was demonstrated [110].

Alternatively, the spin-wave phase was proposed to be used for digitizing information instead of the amplitude (see review [237]). A wave with some chosen phase ϕ_0 corresponds to logic ‘0’ while logic ‘1’ represents the wave with phase $\phi_0 + \pi$. Such an approach allows the trivial embedding of a NOT logic element in magnonic circuits by changing the position of the read-out device by a distance equal to half the wavelength. Moreover, it opens up access to the realization of a majority logic gate in the form of a multi-input spin-wave combiner [109, 191, 238–243]. The spin-wave majority gate consists of three input waveguides where spin waves are excited, a spin-wave combiner which merges the different input waveguides, and an output waveguide where a spin wave propagates with the same phase as the majority of the input waves. Furthermore, this device can perform not only majority operations but also AND and OR operations if one of its inputs is used as a control input [237, 239]. Recently, an experimental prototype of the three-input majority gate was realized and characterized [243]. It was proven that, in accordance with predictions from numerical simulations, the phase of the output signal represents the majority of the phase of the input signals. A switching time of about 10 ns in the prototype evidences the ability of sub-nanosecond data processing in future micro-scaled devices.

The first micro-scale design of the majority gate was demonstrated using micromagnetic simulations in [239]. One of the main problems of a realistic spin-wave majority gate is the coexistence of different spin-wave modes with different wavelengths at a fixed frequency. By choosing the proper width of the output waveguide, it was possible to select the first width mode from the combiner and to ensure the readability of the

output signal. Still, the output signal in [239] was influenced by exchange spin waves of the same frequency but much shorter wavelengths. To overcome these limitations, isotropic forward-volume magnetostatic spin waves were used in [240]. Moreover, a high spin-wave transmission through the gate of up to 64%, which is about three times that for an in-plane magnetized gate, was achieved [240]. A new asymmetric design of the majority gate has been proposed for this purpose. Another promising solution, which is under investigation at the moment, is the application of magnon crystals for spin-wave mode selection in both in-plane and out-of-plane geometries.

An important advantage of the majority gate is that it might operate with spin waves of different wavelengths simultaneously, paving the way toward single-chip parallel computing. This approach requires the splitting of spin-wave signals having different wavelengths and, therefore, the use of magnonic crystals is of crucial importance here [109].

5.6. Magnon transistor

The drawback of electric-current-controlled spin-wave logic devices [110, 234–236, 244] is that it is impossible to combine two logic gates without additional magnon-to-voltage and voltage-to-magnon converters. This fact stimulated the search for means to control a magnon current by another magnon current. Recently, it has been demonstrated that such control is possible owing to nonlinear magnon–magnon scattering, and a magnon transistor allowing all-magnon data processing has been realized (see figure 9) [108]. In this three-terminal device, the density of the magnon current flowing from the source to the drain (see blue spheres in the inset of figure 9(b)) is determined by the amount of magnons injected into the gate of the transistor (red spheres). A magnonic crystal in the form of an array of surface grooves is used to increase the density of the gate magnons and, consequently, to enhance the efficiency of the nonlinear four-magnon scattering process used to suppress the source-to-drain magnon current. It was shown that the source-to-drain magnon current can be decreased by up to three orders of magnitude (see bottom panel in figure 9(b)) [108]. Although the operational characteristics of the presented insulator-based transistor in its proof-of-principle-type

form do not exceed those of semiconductor devices, the presented transistor might play an important role in future magnonic technologies, in which information will be carried and processed by magnons [9].

For example, two magnon transistors embedded into the arms of the Mach–Zehnder interferometer allow one to realize an XOR gate, as shown in figure 9(c). Initially, the feeding magnon current, which is sent to the interferometer, is divided into two identical currents. These currents are injected to the transistors' sources S_1 and S_2 and are independently controlled by the input magnon signals $I_1 = n_{G_1}$ and $I_2 = n_{G_2}$ applied to the gates G_1 and G_2 . The input signal $I = '1'$ corresponds to the critical gate magnon density n_G^{crit} high enough to decrease the magnon density at the drain to a value $n_D/n_{D_0} \leq 1/3$ (see figure 9(b)); an input $I = '0'$ means the absence of gate magnons (the transistor is open). In the case where both input signals are zero $I_1 = I_2 = '0'$, the output signal O after the combiner has a value of '0' due to destructive interference (see the permanent $\pi/2$ phase shift which appears twice in figure 9(c)). The application of a signal to only one of the transistors switches OFF one of the magnon currents and therefore switches OFF destructive interference, resulting in $O = '1'$. Finally, switching OFF both currents results in the absence of magnons at the devices' output $O = '0'$ (see the truth table in figure 9(c)).

6. Summary

Magnonic crystals are artificial magnetic media whose magnetic properties are characterized by periodic variation in space. Bragg scattering affects the spin-wave spectrum in such a periodic structure and leads to the formation of band gaps—frequencies at which spin-wave propagation is prohibited. Consequently, the areas between the band gaps allow for selective spin-wave propagation, whereas pronounced changes of the spin-wave dispersion near the band gap edges cause the formation of band gap solitons, the deceleration of spin waves, and the appearance of confined spin-wave modes. Magnonic crystals are rapidly gaining recognition as structures which have a lot to contribute not only to the study and technological application of spin waves, but also to our general understanding of complex wave dynamics.

In the following, the main fundamental and applied scientific research achievements presented in this article are summarized.

- A new technology based on photolithographic patterning followed by hot orthophosphoric acid etching was developed for the fabrication of groove-based YIG magnonic crystals [153]. The propagation of BVMSWs in such crystals was studied and a high efficiency in the formation of band gaps was observed [153]. The rejection efficiency and the width of the band gaps were studied systematically as a function of groove depth and width as well as the number of grooves.
- It was observed that the rejection efficiency of MSSWs in groove-based magnonic crystals is strongly suppressed

(up to 600 times) compared to the scattering of BVMSWs [200]. It was suggested that this is related to the nonreciprocal nature of the MSSW mode as well as to the resonant scattering of the lowest BVMSW mode into higher thickness modes.

- A technology for the fabrication of YIG structures of micrometer sizes was developed and the spin-wave propagation in a micro-scaled YIG waveguide was investigated [125]. The waveguide was fabricated using e-beam lithography with subsequent Ar^+ ion etching. The spin waves were detected by Brillouin light scattering spectroscopy. It was shown that the mean free path of spin waves in micro-structured YIG reaches at least 31 μm , which is much longer than that in analogous metallic structures.
- A width-modulated micro-scaled permalloy magnonic crystal was developed and studied [134]. The experimental study of the propagation of artificially excited spin waves through a micro-scaled magnonic crystal was performed. The formation of pronounced band gaps in the spin-wave spectrum was demonstrated.
- It was shown, by means of numerical simulations, that the nature of single or multiple band gaps is defined by choosing a sinusoidal or step-like variation of the width of the spin-wave waveguide, respectively [205]. This creates an additional degree of freedom in the control of magnonic crystal properties.
- Ion implantation of a permalloy spin-wave waveguide for the realization of a magnonic crystal with a periodic variation of the saturation magnetization was accomplished [137]. The appearance of clearly defined band gaps was shown, which is due to the absence of the parasitic excitation of higher-order width spin-wave modes in the waveguide. The spin-wave dynamics in such crystals was studied in detail using numerical simulations [208].
- Reconfigurable magnonic crystals based on two-dimensional laser-induced heating with corresponding magnetization patterns were realized [202]. This approach, in contrast to all other existing techniques, opens up access to full dynamic control of the magnetic properties in two dimensions.
- The first dynamic magnonic crystal was realized using an electric-current-carrying meander structure placed in the vicinity of the spin-wave waveguide [219]. It was shown that the characteristics of the crystal are defined by the magnitude of the DC. It was demonstrated that the crystal can be switched ON and OFF faster than 10 ns, which is up to 30 times as fast as the spin-wave relaxation time and the time of spin-wave propagation through the crystal.
- Another approach for the realization of a dynamic magnonic crystal based on a width-modulated spin-wave waveguide was proposed and used for the realization of an AND logic gate for the processing of digital data [110].
- SAWs were used for the scattering of spin waves and to realize a traveling magnonic crystal [221]. The scattering

of BVMSWs with negative group velocity was investigated and a reverse Doppler shift of the frequencies of the scattered waves was observed [221].

- A cumulative achievement is that it was demonstrated that practically any physical parameter that determines spin-wave properties can be varied periodically in space in order to realize a magnonic crystal. Particular parameters which were varied are (i) the spin-wave waveguide thickness [153], (ii) the spin-wave waveguide width [134], (iii) the saturation magnetization of the waveguide [137], (iv) mechanical stress [221], (v) the biasing magnetic field [219] and (vi) the temperature [202].
- The various accomplishments of our research show that magnonic crystals can be used as a micro-scaled microwave filter with tunable characteristics [10, 110, 134, 137, 153, 200–202, 205, 208, 219].
- A magnonic crystal was used as a resonator in order to set the wavenumber and thus to enhance the stability of microwave signal generation based on a feedback loop system [102].
- The coupling of two counter-propagating spin-wave modes [105] as well as frequency inversion and time reversal was realized for the first time using a dynamic magnonic crystal [104]. These results are of importance for wave-based physics as a whole, since they demonstrate that typically nonlinear wave phenomena can be realized in all-linear but dynamic systems.
- The phenomenon of coherent wave trapping and restoration was demonstrated in a groove-based magnonic crystal [106]. Unlike the conventional scheme used in photonics, the trapping occurs not due to the deceleration of the incident wave when it enters the periodic structure but due to the excitation of quasi-normal modes of the artificial crystal. Restoration of the traveling wave was implemented by means of phase-sensitive parametric amplification of the stored mode.
- It is shown that a width-modulated dynamic magnonic crystal can be used as an AND logic gate.
- Two different designs of a micro-scaled majority gate for the processing of digital information were proposed and studied using numerical simulations [239, 240] and experimentally [243]. Their functionality was proven. Magnonic crystals allow for spin-wave filtering in such devices and therefore open up access to parallel computing, in which devices operate simultaneously with linear superposition of spin waves of different wavelengths.
- A groove-based magnonic crystal was used to enhance nonlinear magnon–magnon interactions, and for the realization of magnon-by-magnon control. This resulted in the development of a magnon transistor [108]. It was shown that the density of magnons flowing from the transistor's source to its drain can be decreased by three orders of magnitude through the injection of magnons into the transistor's gate connected to the magnonic crystal.

Acknowledgments

The majority of our results presented in this article were obtained within the framework of the DFG project 'Linear and non-linear magnonic crystals' (SE 1771/1) in close collaboration with B Lagel and S Wolff (Nano Structuring Center, University of Kaiserslautern), M Vogel and G von Freymann (Group of Optical Technologies and Photonics, University of Kaiserslautern), M P Kostylev (University of Western Australia), V S Tiberkevich and A N Slavin (Oakland University), A D Karenowska and J F Gregg (University of Oxford), P Dhagat and A Jander (Oregon State University), the groups of B A Kalinikos (St. Petersburg Electrotechnical University), and J Fassbender (Helmholtz–Zentrum Dresden–Rossendorf). A V Chumak also acknowledges financial support from ERC Starting Grant 678309 MagnonCircuits, A A Serga acknowledges financial support from DAAD (Projekt 57213643, 'Linear and nonlinear spin-wave dynamics in magnonic-crystal-based micro-sized magnon conduits'), and B Hillebrands acknowledges support from the DFG within the framework of SFB/TRR 173: SPIN+X.

References

- [1] Reed K W, Owens J M and Carter R L 1985 *Circuits Syst. Signal Process.* **4** 157
- [2] Hartemann P 1984 *IEEE Trans. Magn.* **20** 1272
- [3] Gubbiotti G, Tacchi S, Madami M, Carlotti G, Adeyeye A O and Kostylev M P 2010 *J. Phys. D: Appl. Phys.* **43** 264003
- [4] Kim S-K 2010 *J. Phys. D: Appl. Phys.* **43** 264004
- [5] Lenk B, Ulrichs H, Garbs F and Munzenberg M 2011 *Phys. Rep.* **507** 107136
- [6] Al-Wahsha H, Akjouj A, Djafari-Rouhani B and Dobrzynski L 2011 *Surf. Sci. Rep.* **66** 29
- [7] Krawczyk M and Grundler D 2014 *J. Phys.: Condens. Matter* **26** 123202
- [8] Serga A A, Chumak A V and Hillebrands B 2010 *J. Phys. D: Appl. Phys.* **43** 264002
- [9] Chumak A V, Vasyuchka V I, Serga A A and Hillebrands B 2015 *Nat. Phys.* **11** 453
- [10] Chumak A V, Karenowska A D, Serga A A and Hillebrands B 2012 The dynamic magnonic crystal: new horizons in artificial crystal based signal processing *Topics in Applied Physics (Magnonics from Fundamentals to Applications* vol 125) ed S O Demokritov and A N Slavin (Berlin: Springer) pp 243–55
- [11] Karenowska A D, Chumak A V, Serga A A and Hillebrands B 2015 Magnon spintronics *Handbook of Spintronics* ed Y Xu et al (Berlin: Springer) pp 1505–49
- [12] Bloch F 1930 *Z. Phys.* **61** 206
- [13] Gurevich A G and Melkov G A 1996 *Magnetization Oscillations and Waves* (New York: CRC Press)
- [14] Stancil D D and Prabhakar A 2009 *Spin Waves: Theory and Applications* (New York: Springer)
- [15] Kalinikos B A, Kovshikov N G and Slavin A N 1983 *Sov. Phys.—JETP Lett.* **38** 413
- [16] Serga A A, Demokritov S O, Hillebrands B and Slavin A N 2004 *Phys. Rev. Lett.* **92** 117203
- [17] Schneider T, Serga A A, Chumak A V, Sandweg C W, Trudel S, Wolff S, Kostylev M P, Tiberkevich V S, Slavin A N and Hillebrands B 2010 *Phys. Rev. Lett.* **104** 197203

- [18] Demidov V E, Demokritov S O, Birt D, O’Gorman B, Tsoi M and Li X 2009 *Phys. Rev. B* **80** 014429
- [19] Gieniusz R, Ulrichs H, Bessonov V D, Guzowska U, Stognii A I and Maziewski A 2013 *Appl. Phys. Lett.* **102** 102409
- [20] Melkov G A, Serga A A, Tiberkevich V S, Oliynyk A N and Slavin A N 2000 *Phys. Rev. Lett.* **84** 3438
- [21] Serga A A, Hillebrands B, Demokritov S O, Slavin A N, Wierzbicki P, Vasyuchka V I, Dzyapko O and Chumak A V 2005 *Phys. Rev. Lett.* **94** 167202
- [22] Demokritov S O, Demidov V E, Dzyapko O, Melkov G A, Serga A A, Hillebrands B and Slavin A N 2006 *Nature* **443** 430
- [23] Serga A A et al 2014 *Nat. Commun.* **5** 3452
- [24] Bozhko D A, Serga A A, Clausen P, Vasyuchka V I, Heussner F, Melkov G A, Pomyalov A, L’vov V S and Hillebrands B 2016 *Nat. Phys.* **12** 1057
- [25] Stamps R L, Breikreutz S J, Chumak A V, Otani Y, Bauer G E W, Thiele J-U, Bowen M, Majetich S A and Kläui M 2014 *J. Phys. D: Appl. Phys.* **47** 333001
- [26] Kruglyak V V and Hicken R J 2006 *J. Magn. Magn. Mater.* **306** 191
- [27] Kruglyak V V, Demokritov S O and Grundler D 2010 *J. Phys. D: Appl. Phys.* **43** 264001
- [28] Nikitov S A, Tailhades P and Tsai C S 2001 *J. Magn. Magn. Mater.* **236** 320
- [29] Skyes C G, Adam J D and Collins J H 1976 *Appl. Phys. Lett.* **29** 388
- [30] Ishak W S 1988 *Proc. IEEE* **76** 171
- [31] Kuchko A N, Sokolovskii M L and Kruglyak V V 2005 *Physica B* **370** 73
- [32] Chi K H, Zhu Y and Tsai C S 2014 *J. Appl. Phys.* **115** 17D125
- [33] Di K, Zhang V L, Kuok M H, Lim H S, Ng S C, Narayanapillai K and Yang H 2014 *Phys. Rev. B* **90** 060405
- [34] Morozova M A, Grishin S V, Sadovnikov A V, Romanenko D V, Sharaevskii Y P and Nikitov S A 2015 *Appl. Phys. Lett.* **107** 242402
- [35] Xing D S, Yang H and Cao Y J 2015 *J. Magn. Magn. Mater.* **377** 286
- [36] Filimonov Y, Pavlov E, Vystostkii S and Nikitov S 2012 *Appl. Phys. Lett.* **101** 242408
- [37] Shindou R, Matsumoto R and Murakami S 2013 *Phys. Rev. B* **87** 174427
- [38] Verba R, Tiberkevich V, Bankowski E, Meitzler T, Melkov G and Slavin A 2013 *Appl. Phys. Lett.* **103** 082407
- [39] Huber R, Krawczyk M, Schwarze T, Yu H, Duerr G, Albert S and Grundler D 2013 *Appl. Phys. Lett.* **102** 012403
- [40] Lisenkov I, Kalyabin D and Nikitov S 2013 *Appl. Phys. Lett.* **103** 202402
- [41] Montoncello F, Tacchi S, Giovannini L, Madami M, Gubbiotti G, Carlotti G, Sirotkin E, Ahmad E, Ogrin F Y and Kruglyak V V 2013 *Appl. Phys. Lett.* **102** 202411
- [42] Lisenkov I, Tyberkevych V, Slavin A, Bondarenko P, Ivanov B A, Bankowski E, Meitzler T and Nikitov S 2014 *Phys. Rev. B* **90** 104417
- [43] Mruczkiewicz M, Pavlov E S, Vysotsky S L, Krawczyk M, Filimonov Y A and Nikitov S A 2014 *Phys. Rev. B* **90** 174416
- [44] Lisenkov I, Tyberkevych V, Nikitov S and Slavin A 2016 *Phys. Rev. B* **93** 214441
- [45] Sadovnikov A V, Beginin E N, Morozova M A, Sharaevskii Yu P, Grishin S V, Sheshukova S E and Nikitov S A 2016 *Appl. Phys. Lett.* **109** 042407
- [46] Morozova M A, Sharaevskaya A Y, Matveev O V, Beginin E N and Sharaevskii Y P 2016 *Phys. Wave Phenom.* **24** 1
- [47] Morozova M A, Matveev O V and Sharaevskii Y P 2016 *Phys. Solid State* **58** 1967
- [48] Ustinov A B, Grigor’eva N V and Kalinikos B A 2008 *JETP Lett.* **88** 31
- [49] Grishin S V, Beginin E N, Sharaevskii Y P and Nikitov S A 2013 *Appl. Phys. Lett.* **103** 022408
- [50] Sheshukova S E, Morozova M A, Beginin E N, Sharaevskii Y P and Nikitov S A 2013 *Phys. Wave Phenom.* **21** 304
- [51] Ustinov A B, Kalinikos B A, Demidov V E and Demokritov S O 2010 *Phys. Rev. B* **81** 180406
- [52] Vysotskii S L, Nikitov S A and Filimonov Y A 2005 *J. Exp. Theor. Phys.* **101** 547
- [53] Keatley P S, Kruglyak V V, Neudert A, Galaktionov E A, Hicken R J, Childress J R and Katine J A 2008 *Phys. Rev. B* **78** 214412
- [54] Tacchi S, Madami M, Gubbiotti G, Tanigawa H, Ono T and Kostylev M P 2010 *Phys. Rev. B* **82** 024401
- [55] Ulrichs H, Lenk B and Muenzenberg M 2010 *Appl. Phys. Lett.* **97** 092506
- [56] Tacchi S et al 2011 *Phys. Rev. Lett.* **107** 127204
- [57] Duerr G, Madami M, Neusser S, Tacchi S, Gubbiotti G, Carlotti G and Grundler D 2011 *Appl. Phys. Lett.* **99** 202502
- [58] Verba R, Melkov G, Tiberkevich V and Slavin A 2012 *Phys. Rev. B* **85** 014427
- [59] Bespalov A V, Golikova O L, Savin S S, Stognij A I and Novitskii N N 2012 *Inorg. Mater.* **48** 1190
- [60] Tacchi S, Duerr G, Klos J W, Madami M, Neusser S, Gubbiotti G, Carlotti G, Krawczyk M and Grundler D 2012 *Phys. Rev. Lett.* **109** 137202
- [61] Saha S, Mandal R, Barman S, Kumar D, Rana B, Fukuma Y, Sugimoto S, Otani Y and Barman A 2013 *Adv. Funct. Mater.* **23** 2378
- [62] Kostylev M, Zhong S, Ding J and Adeyeye A O 2013 *J. Appl. Phys.* **114** 113910
- [63] Han D S, Vogel A, Jung H, Lee K S, Weigand M, Stoll H, Schütz G, Fischer P, Meier G and Kim S K 2013 *Sci. Rep.* **3** 2262
- [64] Chi K H, Zhu Y and Tsai C S 2013 *IEEE Trans. Magn.* **49** 1000
- [65] Liu X M, Ding J, Kakazei G N and Adeyeye A O 2013 *Appl. Phys. Lett.* **103** 062401
- [66] Van de Wiele B and Montoncello F 2014 *J. Phys. D: Appl. Phys.* **47** 315002
- [67] Rodríguez-González B, Bran C, Warnatz T, Rivas J and Vazquez M 2014 *J. Appl. Phys.* **115** 133904
- [68] Wang Q, Zhang H, Tang X, Su H, Bai F, Jing Y and Zhong Z 2014 *J. Phys. D: Appl. Phys.* **47** 065004
- [69] Zivieri R, Malago P and Giovannini L 2014 *Photon. Nanostruct.: Fundam. Appl.* **12** 398
- [70] Malago P, Giovannini L, Zivieri R, Gruszecki P and Krawczyk M 2015 *Phys. Rev. B* **92** 064416
- [71] Kumar D and Adeyeye A O 2015 *J. Appl. Phys.* **117** 143901
- [72] Behncke C, Hanze M, Adolff C F, Weigand M and Meier G 2015 *Phys. Rev. B* **91** 224417
- [73] Tacchi S, Gruszecki P, Madami M, Carlotti G, Klos J W, Krawczyk M, Adeyeye A and Gubbiotti G 2015 *Sci. Rep.* **5** 10367
- [74] Kakazei G N, Liu X M, Ding J, Golub V O, Salyuk O Y, Verba R V, Bunyaev S A and Adeyeye A O 2015 *Appl. Phys. Lett.* **107** 232402
- [75] Odintsov S A, Sadovnikov A V, Grachev A A, Beginin E N, Sharaevskii Y P and Nikitov S A 2016 *JETP Lett.* **104** 563
- [76] Lisenkov I, Tyberkevych V, Levin-Pompetzki L, Elena B, Meitzler T, Nikitov S and Slavin A 2016 *Phys. Rev. Appl.* **5** 064005
- [77] Tacchi S, Gubbiotti G, Madami M and Carlotti G 2017 *J. Phys.: Condens. Matter* **29** 073001
- [78] Krawczyk M and Puzkarski H 2008 *Phys. Rev. B* **77** 054437
- [79] Mamica S 2013 *J. Appl. Phys.* **114** 043912

- [80] Vivas J R, Mamica S, Krawczyk M and Kruglyak V V 2012 *Phys. Rev. B* **86** 144417
- [81] Gubbiotti G, Tacchi S, Carlotti G, Singh N, Goolaup S, Adeyeye A O and Kostylev M 2007 *Appl. Phys. Lett.* **90** 092503
- [82] Wang Z K, Zhang V L, Lim H S, Ng S C, Kuok M H, Jain S and Adeyeye A O 2009 *Appl. Phys. Lett.* **94** 083112
- [83] Tacchi S, Madami M, Gubbiotti G, Carlotti G, Goolaup S, Adeyeye A O, Singh N and Kostylev M P 2010 *Phys. Rev. B* **82** 184408
- [84] Ding J, Kostylev M and Adeyeye A O 2011 *Phys. Rev. Lett.* **107** 047205
- [85] Mruczkiewicz M, Krawczyk M, Mikhaylovskiy R V and Kruglyak V V 2012 *Phys. Rev. B* **86** 024425
- [86] Beginin E N, Filimonov Y A, Pavlov E S, Vysotskii S L and Nikitov S A 2012 *Appl. Phys. Lett.* **100** 252412
- [87] Ma F S, Lim H S, Zhang V L, Ng S C and Kuok M H 2012 *Nanoscale Res. Lett.* **7** 498
- [88] Mruczkiewicz M, Krawczyk M, Sakharov V K, Khivintsev Y V, Filimonov Y A and Nikitov S A 2013 *J. Appl. Phys.* **113** 093908
- [89] Wang Q, Zhang H, Tang X, Fangohr H, Bar F and Zhong Z 2014 *Appl. Phys. Lett.* **150** 112405
- [90] Vysotskii S L, Khivintsev Y V, Filimonov Y A, Nikitov S A, Stognii A I and Novitskii N N 2015 *Tech. Phys. Lett.* **41** 1099
- [91] Kanazawa N, Goto T, Hoong J W, Altansargai B and Takagi H 2015 *J. Appl. Phys.* **117** 17E510
- [92] Ma F, Zhou Y, Braun H B and Lew W S 2015 *Nano Lett.* **15** 4036
- [93] Wang X G, Guo G H, Li Z X, Wang D W, Nie Y Z and Tang W 2015 *Eur. Phys. Lett.* **109** 37008
- [94] Troncoso R E, Ulloa C, Pesce Felipe and Nunez A S 2015 *Phys. Rev. B* **92** 224424
- [95] Bessonov V D, Mruczkiewicz M, Gieniusz R, Guzowska U, Maziewski A, Stognij A I and Krawczyk M 2015 *Phys. Rev. B* **91** 104421
- [96] Kostylev M, Schrader P, Stamps R L, Gubbiotti G, Carlotti G, Adeyeye A O, Goolaup S and Singh N 2016 *Appl. Phys. Lett.* **92** 132504
- [97] Ordóñez-Romero C L, Lázcano-Ortiz Z, Drozdovskii A, Kalinikos B, Aguilar-Huerta M, Dominguez-Juarez J L, Lopez-Maldonado G, Qureshi N, Kolokotsev O and Monsivais G 2016 *J. Appl. Phys.* **120** 043901
- [98] Ustinova I A, Nikitin A A and Ustinov A B 2016 *Tech. Phys.* **61** 473
- [99] Inoue M, Baryshev A, Takagi H, Lim P B, Hatafuku K, Noda J and Togo K 2011 *Appl. Phys. Lett.* **98** 132511
- [100] Kryshnal R G and Medved A V 2012 *Appl. Phys. Lett.* **100** 192410
- [101] Atalay S, Kaya A O, Kolat V S, Gencer H and Izgi T 2015 *J. Supercond. Nov. Magn.* **28** 2071
- [102] Karenowska A D, Chumak A V, Serga A A, Gregg J F and Hillebrands B 2010 *Appl. Phys. Lett.* **96** 082505
- [103] Bankowski E, Meitzler T, Khymyn R S, Tiberkevich V S, Slavin A N and Tang H X 2015 *Appl. Phys. Lett.* **107** 122409
- [104] Chumak A V, Tiberkevich V S, Karenowska A D, Serga A A, Gregg J F, Slavin A N and Hillebrands B 2010 *Nat. Commun.* **1** 141
- [105] Karenowska A D, Gregg J F, Tiberkevich V S, Slavin A N, Chumak A V, Serga A A and Hillebrands B 2012 *Phys. Rev. Lett.* **108** 015505
- [106] Chumak A V, Vasyuchka V I, Serga A A, Kostylev M P, Tiberkevich V S and Hillebrands B 2012 *Phys. Rev. Lett.* **108** 257207
- [107] Ustinov A B, Drozdovskii A V and Kalinikos B A 2010 *Appl. Phys. Lett.* **96** 142513
- [108] Chumak A V, Serga A A and Hillebrands B 2014 *Nat. Commun.* **5** 4700
- [109] Khitun A 2012 *J. Appl. Phys.* **111** 054307
- [110] Nikitin A A, Ustinov A B, Semenov A A, Chumak A V, Serga A A, Vasyuchka V I, Lähderanta E, Kalinikos B A and Hillebrands B 2015 *Appl. Phys. Lett.* **106** 102405
- [111] Damon R W and Eshbach J R 1961 *Phys. Chem. Solids* **19** 308
- [112] Kalinikos B A 1980 *IEE Proc.* **127** 4
- [113] Kalinikos B A and Slavin A N 1986 *J. Phys. C: Solid State Phys.* **19** 7013
- [114] Kalinikos B A, Kozhus N V, Kostylev M P and Slavin A N 1990 *J. Phys.: Condens. Matter* **2** 9861
- [115] Geller S and Gilleo M A 1957 *Acta Crystallogr.* **10** 239
- [116] Glass H L and Elliot M T 1976 *J. Cryst. Growth* **34** 285
- [117] Glass H L 1988 *Proc. IEEE* **76** 151
- [118] Cherepanov V, Kolokolov I and L'vov V 1993 *Phys. Rep.* **229** 81
- [119] Sun Y, Song Y-Y, Chang H, Kabatek M, Jantz M, Schneider W, Wu M, Schultheiss H and Hoffmann A 2012 *Appl. Phys. Lett.* **101** 152405
- [120] d'Allivy Kelly O et al 2013 *Appl. Phys. Lett.* **103** 082408
- [121] Yu H, d'Allivy Kelly O, Cros V, Bernard R, Bortolotti P, Anane A, Brandl F, Huber R, Stasinopoulos I and Grundler D 2014 *Sci. Rep.* **4** 6848
- [122] Hahn C et al 2014 *Appl. Phys. Lett.* **104** 152410
- [123] Onbasli M C, Kehlberger A, Kim D H, Jakob G, Kläui M, Chumak A V, Hillebrands B and Ross C A 2014 *Appl. Phys. Lett. Mater.* **2** 106102
- [124] Liu T, Chang H, Vlaminck V, Sun Y, Kabatek M, Hoffmann A, Deng L and Wu M 2014 *J. Appl. Phys.* **115** 17A501
- [125] Pirro P, Brächer B, Chumak A V, Lägél B, Dubs C, Surzhenko O, Görnert P, Leven B and Hillebrands B 2014 *Appl. Phys. Lett.* **104** 012402
- [126] Dubs C, Surzhenko O, Linke R, Danilewsky A, Brückner U and Dellith J 2017 *J. Phys. D: Appl. Phys.* **50** 204005
- [127] Arnold H D and Elmen G W 1923 *J. Franklin Inst.* **195** 621
- [128] Patton C E 1968 *J. Appl. Phys.* **39** 3060
- [129] Kalarickal S S, Krivosik P, Wu M, Patton C E, Schneider M L, Kabos P, Silva T J and Nibarger J P 2006 *J. Appl. Phys.* **99** 093909
- [130] Demidov V E, Kostylev M P, Rott K, Krzysteczko P, Reiss G and Demokritov S O 2009 *Appl. Phys. Lett.* **95** 112509
- [131] Schwarze T, Huber R, Duerr G and Grundler D 2012 *Phys. Rev. B* **85** 134448
- [132] Vogt K, Fradin F Y, Pearson J E, Sebastian T, Bader S D, Hillebrands B, Hoffmann A and Schultheiss H 2014 *Nat. Commun.* **5** 3727
- [133] Brächer T, Pirro P, Meyer T, Heussner F, Lägél B, Serga A A and Hillebrands B 2014 *Appl. Phys. Lett.* **104** 202408
- [134] Chumak A V et al 2009 *Appl. Phys. Lett.* **95** 262508
- [135] Demidov V E and Demokritov S O 2015 *IEEE Trans. Magn.* **51** 0800215
- [136] Sebastian T, Schultheiss K, Obry B, Hillebrands B and Schultheiss H 2015 *Cond. Matter. Phys.* **3** 35
- [137] Obry B, Pirro P, Brächer B, Chumak A V, Osten J, Ciubotaru F, Serga A A, Fassbender J and Hillebrands B 2013 *Appl. Phys. Lett.* **102** 202403
- [138] Brunsh A 1979 *J. Appl. Phys.* **50** 7603
- [139] Liu X, Zhang W, Carter M J and Xiao G 2011 *J. Appl. Phys.* **110** 033910
- [140] Xu F, Huang Q, Liao Z, Li S and Ong K 2012 *J. Appl. Phys.* **111** 07A304
- [141] Conca A, Greser J, Sebastian T, Klingler S, Obry B, Leven B and Hillebrands B 2013 *J. Appl. Phys.* **113** 213909
- [142] Conca A, Papaioannou E T, Klingler S, Greser J, Sebastian T, Leven B, Lösch J and Hillebrands B 2014 *Appl. Phys. Lett.* **104** 182407

- [143] Heusler F 1903 *Verh. Dtsch. Phys. Ges.* **12** 219
- [144] de Groot R A, Mueller F M, van Engen P G and Buschow K H J 1983 *Phys. Rev. Lett.* **50** 2024
- [145] Kubota T, Tsunegi S, Oogane M, Mizukami S, Miyazaki T, Naganuma H and Ando Y 2009 *Appl. Phys. Lett.* **94** 122504
- [146] Liu C, Mewes C K A, Chshiev M, Mewes T and Butler W H 2009 *Appl. Phys. Lett.* **95** 022509
- [147] Trudel S, Gaier O, Hamrle J and Hillebrands B 2010 *J. Phys. D: Appl. Phys.* **43** 193001
- [148] Oogane M, Kubota T, Kota Y, Mizukami S, Naganuma H, Sakuma A and Ando Y 2010 *Appl. Phys. Lett.* **96** 252501
- [149] Sebastian T et al 2012 *Appl. Phys. Lett.* **100** 112402
- [150] Pirro P, Sebastian T, Brächer T, Serga A A, Kubota T, Naganuma H, Oogane M, Ando Y and Hillebrands B 2014 *Phys. Rev. Lett.* **113** 227601
- [151] Sparks M 1964 *Ferromagnetic Relaxation Theory* (New York: McGraw-Hill)
- [152] Maeda A and Susaki M 2006 *IEEE Trans. Magn.* **42** 3096
- [153] Chumak A V, Serga A A, Hillebrands B and Kostylev M P 2008 *Appl. Phys. Lett.* **93** 022508
- [154] Daimon S, Iguchi R, Uchida K and Saitoh E 2015 *J. Phys. D: Appl. Phys.* **48** 164014
- [155] Ganguly A K and Webb D C 1975 *IEEE Trans. Microw. Theory Tech.* **MTT-23** 998
- [156] Schneider T, Kostylev M P, Serga A A, Neumann T and Hillebrands B 2008 *Phys. Rev. B* **77** 214411
- [157] Au Y, Ahmad E, Dmytriiev O, Dvornik M, Davison T and Kruglyak V V 2012 *Appl. Phys. Lett.* **100** 182404
- [158] Haiming Y, d'Allivy Kelly O, Cros V, Bernard R, Bortolotti P, Anane A, Brandl F, Heimbach F and Grundler D 2016 *Nat. Commun.* **7** 11255
- [159] Kakazei G N, Mewes T, Wigen P E, Hammel P C, Slavin A N, Pogorelov Yu G, Costa M D, Golub V O, Guslienko K Yu and Novosad V 2008 *J. Nanosci. Nanotechnol.* **8** 2811
- [160] Klingler S, Chumak A V, Mewes T, Khodadadi B, Mewes C, Dubs C, Surzhenko O, Hillebrands B and Conca A 2015 *J. Phys. D: Appl. Phys.* **48** 015001
- [161] Chumak A V, Melkov G A, Demidov V E, Dzyapko O, Safonov V L and Demokritov S O 2009 *Phys. Rev. Lett.* **102** 187205
- [162] Brächer T, Pirro P and Hillebrands B 2016 arXiv:1611.05893
- [163] Kennewell K J, Crew D C, Lwin M J, Woodward R C, Prasad S and Stamps R L 2007 *Surf. Sci.* **601** 5766
- [164] Smith K R, Kabatek M J, Krivosik P and Wu M 2008 *J. Appl. Phys.* **104** 043911
- [165] Demokritov S O, Hillebrands B and Slavin A N 2001 *Phys. Rep.* **348** 441
- [166] Fohr F, Serga A A, Schneider T, Hamrle J and Hillebrands B 2009 *Rev. Sci. Instrum.* **80** 043903
- [167] Sandweg C W, Jungfleisch M B, Vasyuchka V I, Serga A A, Clausen P, Schultheiss H, Hillebrands B, Kreisel A and Kopietz P 2010 *Rev. Sci. Instrum.* **81** 073902
- [168] Kirilyuk A, Kimel A V and Rasing T 2010 *Rev. Mod. Phys.* **82** 2731
- [169] Lambert C-H et al 2014 *Science* **345** 1337
- [170] Bauer G H, Chauleau J Y, Woltersdorf G and Back C H 2014 *Appl. Phys. Lett.* **104** 102404
- [171] Tserkovnyak Y, Brataas A and Bauer G E W 2002 *Phys. Rev. Lett.* **88** 117601
- [172] Costache M V, Sladkov M, Watts S M, van der Wal C H and van Wees B J 2006 *Phys. Rev. Lett.* **97** 216603
- [173] Saitoh E, Ueda M, Miyajima H and Tataru G 2006 *Appl. Phys. Lett.* **88** 182509
- [174] Kajiwara Y et al 2010 *Nature* **464** 262
- [175] Sandweg C W, Kajiwara Y, Chumak A V, Serga A A, Vasyuchka V I, Jungfleisch M B, Saitoh E and Hillebrands B 2011 *Phys. Rev. Lett.* **106** 216601
- [176] Chumak A V, Serga A A, Jungfleisch M B, Neb R, Bozhko D A, Tiberkevich V S and Hillebrands B 2012 *Appl. Phys. Lett.* **100** 082405
- [177] Hoffmann A 2013 *IEEE Trans. Magn.* **49** 5172
- [178] Slonczewski J C 1995 *J. Magn. Magn. Mater.* **159** L1
- [179] Krivorotov I N, Emley N C, Sankey J C, Kiselev S I, Ralph D C and Buhrman R A 2005 *Science* **307** 228
- [180] Demidov V E, Urazhdin S and Demokritov S O 2010 *Nat. Mater.* **9** 984
- [181] Madami M, Bonetti S, Consolo G, Tacchi S, Carlotti G, Gubbiotti G, Mancoff F B, Yar M A and Åkerman J 2011 *Nat. Nanotechnol.* **6** 635
- [182] Demidov V E, Urazhdin S, Ulrichs H, Tiberkevich V, Slavin A, Baither D, Schmitz G and Demokritov S O 2012 *Nat. Mater.* **11** 1028
- [183] Collet M et al 2016 *Nat. Commun.* **7** 10377
- [184] Lauer V et al 2016 *Appl. Phys. Lett.* **108** 012402
- [185] Cornelissen L J, Liu J, Duine R A, Ben Youssef J and van Wees B J 2015 *Nat. Phys.* **11** 1022
- [186] Lauer V et al 2017 *IEEE Magn. Lett.* **8** 3104304
- [187] Plihal M, Mills D L and Kirschner J 1999 *Phys. Rev. Lett.* **82** 2579
- [188] Tang W X, Zhang Y, Tudosa I, Prokop J, Eitzkorn M and Kirschner J 2007 *Phys. Rev. Lett.* **99** 087202
- [189] Khitun A and Wang K L 2005 *Superlattices Microstruct.* **38** 184
- [190] Dutta S, Chang S-C, Kani N, Nikonov D E, Manipatruni S, Young I A and Naeemi A 2015 *Sci. Rep.* **5** 9861
- [191] Zografos O et al 2015 *Proc. of the 15th IEEE Int. Conf. on Nanotechnology (Rome, Italy, 27–30 July 2015)* (<https://doi.org/10.1109/ICICDT.2015.7165881>)
- [192] Klein O, de Loubens G, Naletov V V, Boust F, Guillet T, Hurdequint H, Leksikov A, Slavin A N, Tiberkevich V S and Vukadinovic N 2008 *Phys. Rev. B* **78** 144410
- [193] An T et al 2013 *Nat. Mater.* **12** 549
- [194] Bocklage L, Swoboda C, Schlage K, Wille H-C, Dzemiantsova L, Bajt S, Meier G and Röhlberger R 2015 *Phys. Rev. Lett.* **114** 147601
- [195] Goulon J, Rogalev A, Wilhelm F, Jaouen N, Goulon-Ginet C, Goujon G, Youssef J B and Indendom M V 2005 *JETP Lett.* **82** 696
- [196] Martin T, Woltersdorf G, Stamm C, Schlage K, Dürr H A, Mattheis R, Back C H and Bayreuther G 2008 *J. Appl. Phys.* **103** 07B112
- [197] Stenning G B G et al 2015 *New J. Phys.* **17** 013019
- [198] Mihai A P, Attané J P, Marty A, Warin P and Samson Y 2008 *Phys. Rev. B* **77** 060401
- [199] Raquet B, Viret M, Sondergard E, Cespedes O and Mamy R 2002 *Phys. Rev. B* **66** 024433
- [200] Chumak A V, Serga A A, Wolff S, Hillebrands B and Kostylev M P 2009 *Appl. Phys. Lett.* **94** 172511
- [201] Chumak A V, Serga A A, Wolff S, Hillebrands B and Kostylev M P 2009 *J. Appl. Phys.* **105** 083906
- [202] Vogel M, Chumak A V, Waller E H, Langner T, Vasyuchka V I, Hillebrands B and von Freymann G 2015 *Nat. Phys.* **11** 487
- [203] Lee K S, Han D S and Kim S K 2009 *Phys. Rev. Lett.* **102** 127202
- [204] Arikani M, Au Y, Vasile G, Ingvarsson S and Kruglyak V V 2013 *J. Phys. D: Appl. Phys.* **46** 135003
- [205] Ciubotaru F, Chumak A V, Grigoryeva N Yu, Serga A A and Hillebrands B 2012 *J. Phys. D: Appl. Phys.* **45** 255002
- [206] Wang Q, Zhong Z, Jin L, Tang X, Bai F, Zhang H and Beach G S D 2013 *J. Magn. Magn. Mater.* **340** 23
- [207] Wang Q, Zhang H, Ma G, Liao Y, Zheng Y and Zhong Z 2014 *J. Appl. Phys.* **115** 133906
- [208] Ciubotaru F, Chumak A V, Obry B, Serga A A and Hillebrands B 2013 *Phys. Rev. B* **88** 134406
- [209] Topp J, Heitmann D, Kostylev M P and Grundler D 2010 *Phys. Rev. Lett.* **104** 207205

- [210] Morozova M A, Sharaevskii Y P and Nikitov S A 2014 *J. Commun. Technol. Electron.* **59** 467
- [211] Kakazei G N, Liu X M, Ding J and Adeyeye A O 2014 *Appl. Phys. Lett.* **104** 042403
- [212] Ustinov A B and Kailinikos B A 2014 *Tech. Phys. Lett.* **40** 570
- [213] Di K, Lim H S, Zhang V L, Ng S C, Kuok M H, Nguyen H T and Cottam M G 2014 *J. Appl. Phys.* **115** 053904
- [214] Berendt J, Teixeira J M, Garcia-Garcia A, Raposo M, Ribeiro P A, Dubowik J, Kakazei G N and Schmoor D S 2014 *Appl. Phys. Lett.* **104** 082408
- [215] Li Z X, Wang X G, Wang D W, Nie Y Z, Tang W and Guo G H 2015 *J. Magn. Mater.* **338** 10
- [216] Morozova M A, Matveev O V, Sharaevskii Y P and Nikitov S A 2016 *Phys. Solid State* **58** 273
- [217] Wang Q, Chumak A V, Jin L, Zhang H, Hillebrands B and Zhong Z 2017 *Phys. Rev. B* **95** 134433
- [218] Obyr B, Vasyuchka V I, Chumak A V, Serga A A and Hillebrands B 2012 *Appl. Phys. Lett.* **101** 192406
- [219] Chumak A V, Neumann T, Serga A A, Hillebrands B and Kostylev M P 2009 *J. Phys. D: Appl. Phys.* **42** 205005
- [220] Fetisov Y K, Ostrovskaya N V and Popkov A F 1996 *J. Appl. Phys.* **79** 5730
- [221] Chumak A V, Dhagat P, Jander A, Serga A A and Hillebrands B 2010 *Phys. Rev. B* **81** 140404
- [222] Kryshtal R G and Medved A V 2017 *J. Man. Magn. Mater.* **426** 666
- [223] Kryshtal R G and Medved A V 2015 *J. Magn. Mater.* **395** 180
- [224] Stancil D D, Henty B E, Cepni A G and Van't Hof J P 2006 *Phys. Rev. B* **74** 060404
- [225] Kalinikos B A, Kovshikov N G and Patton C E 1998 *Phys. Rev. Lett.* **80** 4301
- [226] Demokritov S O, Serga A A, Demidov V E, Hillebrands B, Kalinikos B A and Kostylev M P 2003 *Nature* **426** 159
- [227] Zel'dovich Ya B, Pilipetsky N F and Shkunov V V 1985 *Principles of Phase Conjugation* (Berlin: Springer)
- [228] Korpel A and Chatterjee M 1981 *Proc. IEEE* **69** 1539
- [229] Sivan Y and Pendry J B 2011 *Opt. Express* **19** 14502
- [230] Krauss T 2007 *J. Phys. D: Appl. Phys.* **40** 2666
- [231] Baba T 2008 *Nat. Photon.* **2** 465
- [232] Serga A A, Chumak A V, Andre A, Melkov G A, Slavin A N, Demokritov S O and Hillebrands B 2007 *Phys. Rev. Lett.* **99** 227202
- [233] Chumak A V, Serga A A, Melkov G A, Tiberkevich V, Slavin A N and Hillebrands B 2009 *Phys. Rev. B* **79** 014405
- [234] Hertel R, Wulfhekel W and Kirschner J 2004 *Phys. Rev. Lett.* **93** 257202
- [235] Kostylev M P, Serga A A, Schneider T, Leven B and Hillebrands B 2005 *Appl. Phys. Lett.* **87** 153501
- [236] Schneider T, Serga A A, Leven B, Hillebrands B, Stamps R L and Kostylev M P 2008 *Appl. Phys. Lett.* **92** 022505
- [237] Khitun A and Wang K L 2011 *J. Appl. Phys.* **110** 034306
- [238] Khitun A, Bao M and Wang K L 2010 *J. Phys. D: Appl. Phys.* **43** 264005
- [239] Klingler S, Pirro P, Brächer T, Leven B, Hillebrands B and Chumak A V 2014 *Appl. Phys. Lett.* **105** 152410
- [240] Klingler S, Pirro P, Brächer T, Leven B, Hillebrands B and Chumak A V 2015 *Appl. Phys. Lett.* **106** 212406
- [241] Ganzhorn A, Klingler S, Wimmer T, Geprägs S, Gross R, Huebl H and Goennenwein S T B 2016 *Appl. Phys. Lett.* **109** 022405
- [242] Brächer T, Heussner F, Pirro P, Meyer T, Fischer T, Geilen M, Heinz B, Lägél B, Serga A A and Hillebrands B 2016 *Sci. Rep.* **6** 38235
- [243] Fischer T, Kewenig M, Bozhko D A, Serga A A, Syvorotka I I, Ciubotaru F, Adelman C, Hillebrands B and Chumak A V 2017 **110** 152401
- [244] Lee K-S and Kim S-K 2008 *J. Appl. Phys.* **104** 053909